Cold Streams in High-Redshift-Galaxies

Adelheid Teklu

München 2012

Cold Streams in High-Redshift-Galaxies

Bachelor Thesis

at

Ludwig–Maximilians–Universität München

submitted by

Adelheid Teklu

(Matr. Nr.: 10058638)

born 3rd of February 1984 in Munich

supervised by
Prof. Dr. Andreas Burkert

and
Dr. Klaus Dolag

Munich, July 25, 2012

Evaluator: Prof. Dr. Andreas Burkert

Day of the oral exam: September 21, 2012

Contents

1. Introduction

Galaxies are very fascinating. One of the reasons for this may be that they have not yet revealed all of their secrets to us. To recognize the real nature of galaxies took a while. At first they were thought to be just nebulae because of their diffuse appearance. In the 18th century (Hetznecker, 2007), when Messier included some galaxies into his catalog he did not know he was looking at objects that were not part of our own Milky Way but rather far away, since he and his colleagues only had their naked eyes and simple telescopes to explore the true nature of these nebulae (Hetznecker, 2007). This might be one of the reasons why the galaxies that were included into catalogs by Messier are named as 'nebulae', for example Andromeda-nebula (which has the entry M31 in the Messier-catalog) or Bode's Nebula (M81 and M82). In 1912, Vesto Slipher used spectroscopic methods to explore these spiral-nebulae and found that they were rotating. Because of this observation a great debate began in 1920 whether the nebulae were a part of the Milky Way or had to be of extragalactic nature. Unlike Harlow Shapley, who said that these nebulae were inside our own galaxy, Heber Curtis claimed that they had to lie outside of the Milky Way (Schneider, 2007). In 1923, the jurist and astronomer Edwin Hubble observed Cepheids in the Andromeda-nebula and by using the period-luminosity-relation he calculated our distance to this nebula. His results revealed that it had to be extragalactic and so this finally ended the debate (Hetznecker, 2007). This marked the birth of extragalactic astronomy.

In 1933, Fritz Zwicky studied the rotation-curves of the Coma-Cluster of Galaxies. The visible mass was not enough to explain the flat rotation-curves with v_{rot} remaining constant instead of the expected keplerian fall-off of the rotational velocity $v_{rot} \propto 1/\sqrt{r}$ (Peacock, 1998). To explain this, he concluded that there had to be some mass that could not be seen, and he introduced the idea of 'Dark Matter' (DM) (Hetznecker, 2007). Today we know that the non-baryonic dark matter does not interact electromagnetic but purely gravitational and that the visible components of all galaxies are surrounded by a halo of dark matter. This leads us to the question how galaxies have formed and evolved.

For a better understanding of the formation of galaxies it is appropriate to discuss the evolution of the universe from its beginning, which will be done in the following passage:

The first point in time we can talk about is the Planck time at about 10^{-43}s. About everything that happened before the Planck time only speculations can be made. The beginning of the universe where all the energy and matter is concentrated, is known as 'Big Bang'. At that time, when the primordial soup is about 10^{32}K hot, radiation and matter are in equilibrium and the four fundamental forces are probably unified. Since the expansion has lowered the temperature, the gravitational force decouples about 10^{-35}s after the Planck time. Quarks, leptons, the force carriers and their antiparticles 'live' in permanent annihilation and creation, while the gravitational force slows down the expansion (Hetznecker, 2007). Then the strong interaction force decouples from the weak, which could have caused a phase transition at quantum-fluctuations. This leads to an enormous energy density, when the universe is about 10^{-33}s old (Weigert et al., 2009). The following inflation makes the universe grow from the size of an atom-nucleus to the dimension of our solar system and lasts about 10^{-33}s (Hetznecker, 2007). After that the normal expansion cools down the temperature and so finally at about 10^{-10}s the electromagnetic and the weak interaction decouple from each other.
Now that the fundamental forces are separated, quarks can build baryons and other heavy particles (Weigert et al., 2009). When the universe is 1 s old, most of the electron-positron-pairs annihilate, the neutrinos decouple because the interactions have become inefficient and so the neutrons and protons can form nuclei, which get instantly destroyed by the photons. At this time the dark matter decouples, which is an important aspect for the structure formation that follows. As time goes by, the universe expands and so the temperature continues to drop, so that at about 3 s stable atom-nuclei are built during the so called primordial nucleosynthesis. Now the matter consists of ionized plasma where the still high-energetic photons prevent a stable binding between the electrons and the nuclei. Due to the expansion the density decreases and the photons lose energy because of the redshift and so the H- and He-nuclei can recombine with the free electrons without being separated again. The plasma becomes a neutral gas and since there are no interactions between the atoms and the radiation, the photons decouple from matter. This takes place about 380000 ($z \approx 1100$) years after the big bang and is still seen as the Cosmic Microwave Background Radiation (CMBR). The universe has become transparent

for the photons. The following epoch is therefore called the dark ages.

Now the baryons can fall into the potential wells of the dark matter, which have had time to gather because of its gravitational force, built troughs and finally between z≈20 and 10 the first stars must have formed in these dark matter seeds. The UV-radiation of these probably very massive stars (M $\gtrsim$ 10 $M_\odot$) re-ionizes the neutral gas (Binney and Tremaine, 2008). The exact timeline of the reionization is part of the current research (e.g. Bolton et al. (2011)). The reionization-epoch was finished at z≈6 (Binney and Tremaine, 2008), which can be derived from the observation of the absorption spectrum of high redshifted quasars (z>5.7) (Schneider, 2007). At about this point the simulation that we have analyzed begins.

How can we find out, in which way the 'normal' galaxies have formed and evolved? To investigate structure formation, several cosmological simulations have been made, e.g. the Millenium Simulation by Springel et al. (2005b). We want to focus on the question whether galaxies have formed by merging or by cold gas inflow.

Dekel et al. (2009a) investigated halos at different redshifts in a simulation and the connection between narrow streams of cold inflowing gas from the cosmic web and the starformation in these galaxies. They concluded that galaxies of baryonic mass $\sim 10^{11} M_\odot$ at z∼2.5 formed stars at high efficiencies and that most of the stars in the universe are the results of these streams of gas with temperatures $< 10^5$ K feeding halos of mass $> 2 \cdot 10^{11} M_\odot$ between redshift 1.5 and 4. They proposed this cold stream scenario as an alternative to the formation of galaxies by mergers. One argument for it is that these streams do not change the rotating disk configuration.

In this work we want to discuss the analysis of the simulation by Dolag by looking at interesting properties of halos at redshift 2.33. First we will explain some important physical foundations that may be useful for understanding the physics of these halos. Then we will come to present and debate our results. We picked out four halos at one redshift and study e.g. the behavior of pressure, density and finally the relation between massflux and starformation rate over the time and discuss if there is a difference in the formation of spiral galaxies and elliptical galaxies.

2. Theoretical Foundations

2.1. Hierarchical Growth of Halos and Cold Streams along Filaments

In the standard picture of a ΛCDM universe halos grow hierarchically from small density flucutations. As mentioned in the introduction the dark matter decouples very early from the baryonic matter, thus has more time to follow the density fluctuations and become dense due to the gravitational potential. After decoupling from the photons, the baryonic matter gathers along dark matter filaments and the gas condenses in the center of the dark matter halos. This filamentary structure, also called cosmic web, has been studied widely in observations like the Sloan Digital Sky Survey (SDSS) (for example Berlind et al. (2006), see left side of Fig. 2.1) and simulations (for example Springel et al. (2005b), see right side of Fig. 2.1).

When the gas clouds collapse under their gravitation, stars form and these stars build galaxies.

Galaxies can be divided into three main types according to their appearance. This classification is known as the Hubble sequence. In elliptical galaxies the bulge is the dominant component and they are mainly red in the optical. Spiral galaxies consist of a bulge and a disk with spiral arms. The third type are the irregular galaxies, which do not have a structure. The question how these different classes of galaxies have formed is not doubtlessly explained yet (Schneider, 2007).

In a series of papers Dekel et al. (Dekel and Birnboim (2006), Dekel et al. (2009a) and Dekel et al. (2009b)) propose that galaxies are built by streams of cold gas that is flowing in from the filaments of the cosmic web.

The streams can be divided in two main modes, which make a contribution to the structure of the galaxies at later times: The main component of the cold flows consists of smooth gas. There are also gas clumps, which migrate inwards and merge in the halo center. This can be seen in Fig. 2.2, taken from Dekel et al. (2009a).

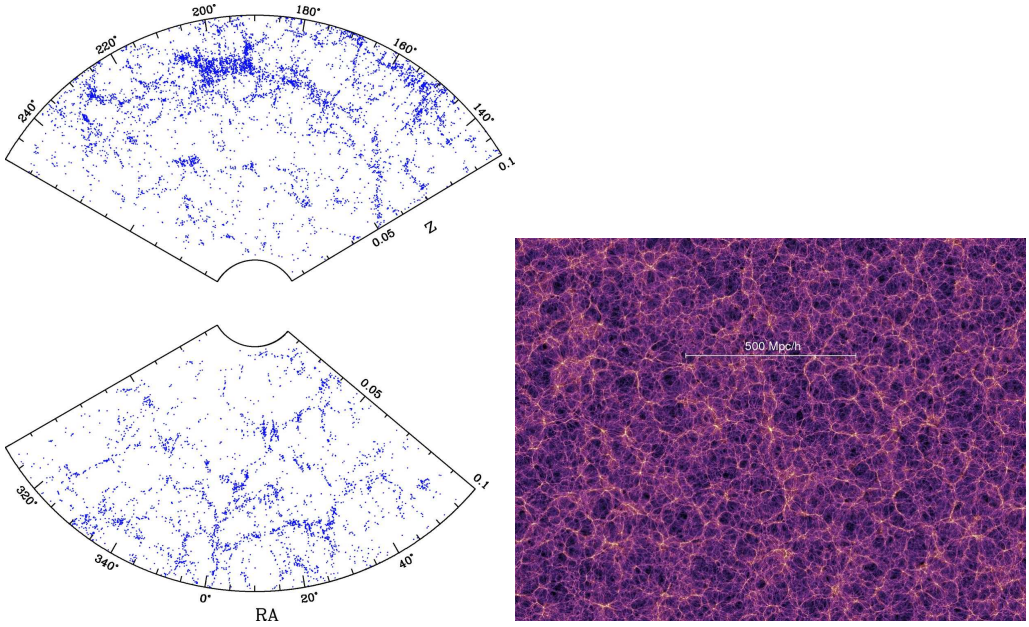

Fig. 2.1.: Left: This fig. is taken from Berlind et al. (2006) and shows the cosmic web from the observations of the SDSS. Right: Millenium Simulation, taken from Springel et al. (2005b) (`http://www.mpa-garching.mpg.de/galform/presse/`), shows the filamentary structure of the universe for z = 0.

If the stream is mainly smooth, the inflowing gas is building up the disk and breaks it into clumps, which trigger the starformation and form compact bulges.

A clumpy stream, on the other hand, perturbs the disk, leads to a high velocity dispersion and builds up a massive bulge. This massive spheroid stabilizes the disk against the formation of disk-clumps and thus suppresses the starformation (Dekel et al., 2009b).

In general, these cold streams cross the medium of the halo, which has been heated by an outwards propagating shock. At $z \geqslant 2$, halos with $M \gtrsim 10^{12} M_{\odot}$ are fed by cold flows, which lead to high starformation rates. At lower redshifts the cold streams break down because the gas is heated by a virial shock and the feedback of the Active Galactic Nucleus (AGN), which is a strong source in the center of an active galaxy, that results from the accretion of material onto a supermassive black hole in the center (for definition of AGN see e.g. Schneider (2007)). Since the cooling rate is slower than the compression rate, the gas cannot cool.

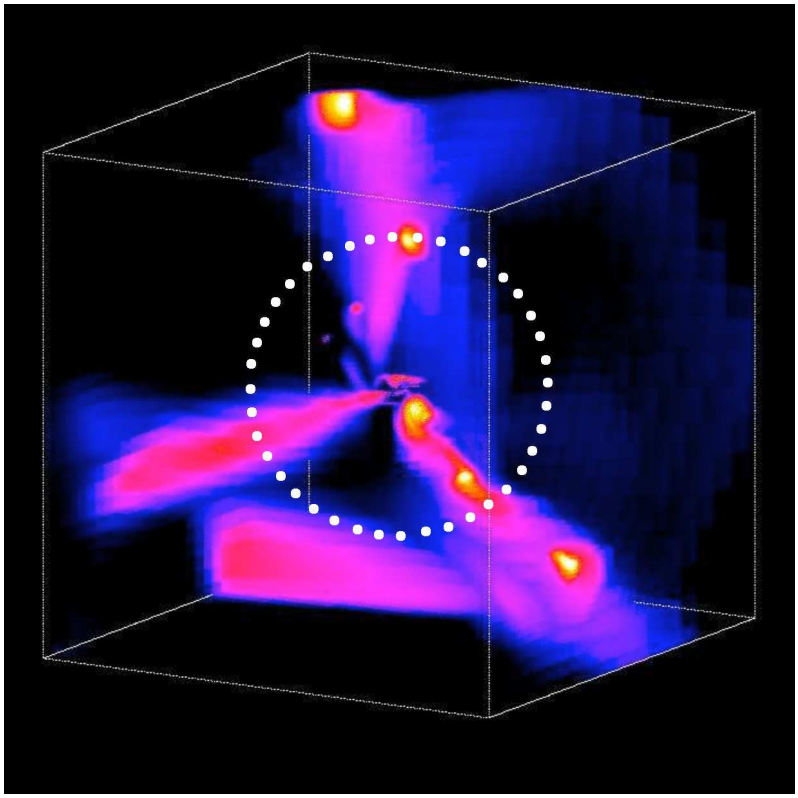

Fig. 2.2.: This picture from a simulation, taken from Dekel et al. (2009a), shows streams in three dimensions. There are smooth and clumpy streams. The virial radius is the white dotted circle.

2.2. Starformation

For a better understanding of the properties of the galaxies and the behavior of the different components of the halos (e.g. pressure relations), we want to explain how stars form in general.

The constraint for the formation of stars is the gravitational collapse. For this the gravitational force has to be higher than the pressure of the gas (Weigert et al., 2009). We assume the molecular cloud to be in hydrostatic equilibrium, which is given by

$$\nabla p = -\rho \nabla \phi \qquad \text{(e.g. Landau and Lifschitz (1991))},$$

Now perturbations can occur, e.g. by a supernova that causes shock waves (Prialnik, 2000) or stars that pass by (Weigert et al., 2009). Such a perturbation distrurbs the hydrostatic equilibrium state of this cloud. The consequence is that there are regions with lower and with higher densities. In the regions of higher density the gravity

will increase. To achieve hydrostatic equilibrium the pressure increases as well.

From the virial theorem

$$2\langle E_{kin}\rangle = -\langle E_{pot}\rangle$$

the condition for the collapse of the region can be derived. (For the derivation see e.g. Carroll and Ostlie (2007).) We get the necessary criterion that the collapse is depending on the Jeans radius

$$R_J = \frac{\alpha}{3}\frac{\mu G M}{\mathcal{R}T},$$

where α is a constant, which takes the mass distribution into account. If the radius is smaller than the Jeans radius the pressure of the gas cannot balance the gravitational force and therefor collapses. We can also express this in dependency of the mass. The critical mass, above which the cloud collapses can be derived from the Jeans radius and is called the Jeans mass

$$M_J = \left[\left(\frac{3}{4\pi}\right)^{1/2}\left(\frac{3}{\alpha}\right)^{3/2}\right]\left(\frac{\mathcal{R}T}{\mu G}\right)^{3/2}\frac{1}{\sqrt{\rho_{av}}} \approx 10^5\frac{T^{3/2}}{\sqrt{n}}M_\odot,$$

where ρ_{av} = M/V and n is the volume number density. When a cloud collapses the density and the temperature increase. If the cooling in the molecular cloud is inefficient, the collapse will only continue if the mass of the cloud is greater than M_J. Should the cooling be efficient, then regions within the cloud can collapse, which leads to a fragmentation of the cloud. When these fragments become denser and thus opaque, the radiative cooling becomes inefficient. Such a fragment is bound by self-gravity due to the density, which leads to a decrease in temperature. This fragment can be seen as the seed of a star, if it lies in the stellar mass range, which lies between 0.08 and 150 $M_\odot$ (Massey and Meyer, 2001). A more detailed description of the starformation and evolution can be found in Prialnik (2000) and Klessen (2007).

2.3. Massflux

Since the starformation rate follows the net cold gas accretion rate (Bouché et al., 2010), we briefly want to derive the mass flow rate that we have used for our calculations. We have parted the radius, which is three times the virial radius (R_{vir}), in 31 tics, so in the formulae the integer i $\in$ [0,30]. The virial radius is defined by

the density of the particles. Within the virial radius the mean density is 200 times higher than the mean critical density of the universe (Carlberg et al., 1997).

We start with the change of volume, which is given by

$$\Delta V = A_i v_i \Delta t \qquad \text{(e.g. Tipler (1994))},$$

where v_i is the radial velocity of the gas particles in the i-th tic and A_i the area that is crossed in time Δt. Here we are interested in the radial velocity, since we only need the particles, that move in direction to the halo center. With V = M/ρ, $\rho = \frac{m_i}{A_i \delta r_i}$, an assumed constant density and a simple algebraic transformation we get

$$\frac{dM}{dt} = \frac{v_i m_i}{\delta r_i}.$$

This is the used formula for the massflux, where m_i is the in- and outflowing mass in the i-th tic and δr_i the section of the radius.

We implemented the mass flow rate by the following steps:

First the radial velocity is calculated by projecting the velocity vector onto the normalized position vector. Then we define the binradius, which is in the middle of two tics on the radius-scale and for that we have 30 entries for the massflux along the radius. The particles now are devided in in- and outflowing ones. For the incoming particles we select those, whose scalarproduct of the radial velocity vector and the position vector are smaller than zero and for the outflowing particles the scalarproduct is greater than zero.

After that the cold particles are seperated from the hot particles. This is done by selecting the gas particles, that have a temperature smaller than 10^5 K. Also particles with a coldfraction greater than zero are counted to the cold gas, because they are about to form stars and in the simulation formally counted to the hot particles. When the gas particles move to the 'starformation-branch', they reach temperatures of 10^5 K and higher. Hence we make the cut between the cold and the hot particles at this limit. Then we implement the massflux formula for the inflowing cold gas particles including the starforming ones and do the same for the outflowing ones as well as for the hot gas particles. The net massflux is defined by the massflux of incoming less the outgoing gas particles.

We will compare our mass flow rate to that assumed in (Dekel et al., 2009a). The

formula in this paper is given by

$$\dot{M} \simeq 6.6 M_{12}^{1.15}(1+z)^{2.25} f_{.165} M_{\odot} yr^{-1},$$

where $M_{12} \equiv \frac{M_{vir}}{10^{12} M_{\odot}}$, and $f_{.165} \equiv \frac{f_{baryon}}{0.165}$ is the baryonic fraction in halo units.

2.4. The Used Simulation

The data that we analyze is taken from the cosmological hydrodynamical simulation Magneticum Pathfinder, which is an extended version of the GADGET-2 code (Springel et al. (2001) and Springel (2005)). A lot of physical effects of the baryonic matter is integrated in this simulation e.g. cooling, starformation, supernova-driven winds (Springel and Hernquist, 2003), chemical enrichment from stellar populations, AGB stars, SNe (Tornatore et al. (2007) and Tornatore et al. (2004)), low viscosity SPH (Dolag et al., 2005), black hole growth and AGN feedback (Springel et al. (2005a) and Fabjan et al. (2010)). The cosmological parameters are h = 0.704, Ω_0 = 0.268, Ω_Λ = 0.728, Ω_b = 0.044 and σ_8 = 0.776 with respect to the 7-year WMAP estimates, given by Komatsu et al. (2011).

The length of box 4 is 48 Mpc/h and has $2 \cdot 576^3$ particles in the ultra high resolution. The mass resolutions are $M_{DM} = 3.6 \cdot 10^7 M_{\odot}/h$ for dark matter particles and $M_{gas} = 7.3 \cdot 10^6 M_{\odot}/h$ for gas particles. In this simulation we have six types of particles. Relevant for our investigations are gas, star, dark matter and black hole particles. Each of the gas particles can form four stars. The starforming particles have a cold fraction greater than zero and a temperature higher than 10^5 K. The simulation is parted into 144 snapshots. Snapshot 032 is redshift 2.33, which we investige first and then we study the halos from snapshot 020 (z = 4.23) to 060 (z = 0.96).

3. Results and Discussion

In the following chapter we want to present the results of our investigations. In section 3.1 we introduce the halos that were picked from the simulation, in section 3.2 we discuss their properties at redshift 2.33 and in section 3.3 we compare the properties at different redshifts.

3.1. Portrait of the Selected Halos

The most efficient starforming galaxies can be found at redshifts 2-3 (Dekel et al., 2009a). To better understand the mechanisms that cause this high starformation rates we study galaxies and their environments chosen from the cosmological simulation introduced in section 2.4 at a redshift of 2.33. Since the halos more massive than $10^{13} M_{\odot}$ mostly host galaxy-clusters and therefore are not suitable for our intentions to reconstruct the formation of a single galaxy, this is chosen as the upper limit of the mass range.

We have chosen the lower mass range according to the results by Dekel et al. (2009a) that most of the efficient starforming galaxies have halo masses greater than $10^{12} M_{\odot}$.

At this redshift most of the 130 halos in the virial mass range from $10^{12} - 10^{13} M_{\odot}$ show streams of cold gas, most of them smooth with small substructures and some with streams that are very clumpy.

To get a better view we have created a list with the most important properties of the four halos, which can be found in the Appendix, A.1 - A.4.

Halo 1 was selected because it has four streams, one of them very narrow. The other three almost lie in a plane. One of these is very clumpy, as seen in Fig. 3.1, where the halos are plotted in three dimensions with a color range for the temperature.

Halo 2 has four streams, two are narrow. There are several clumps, which are not

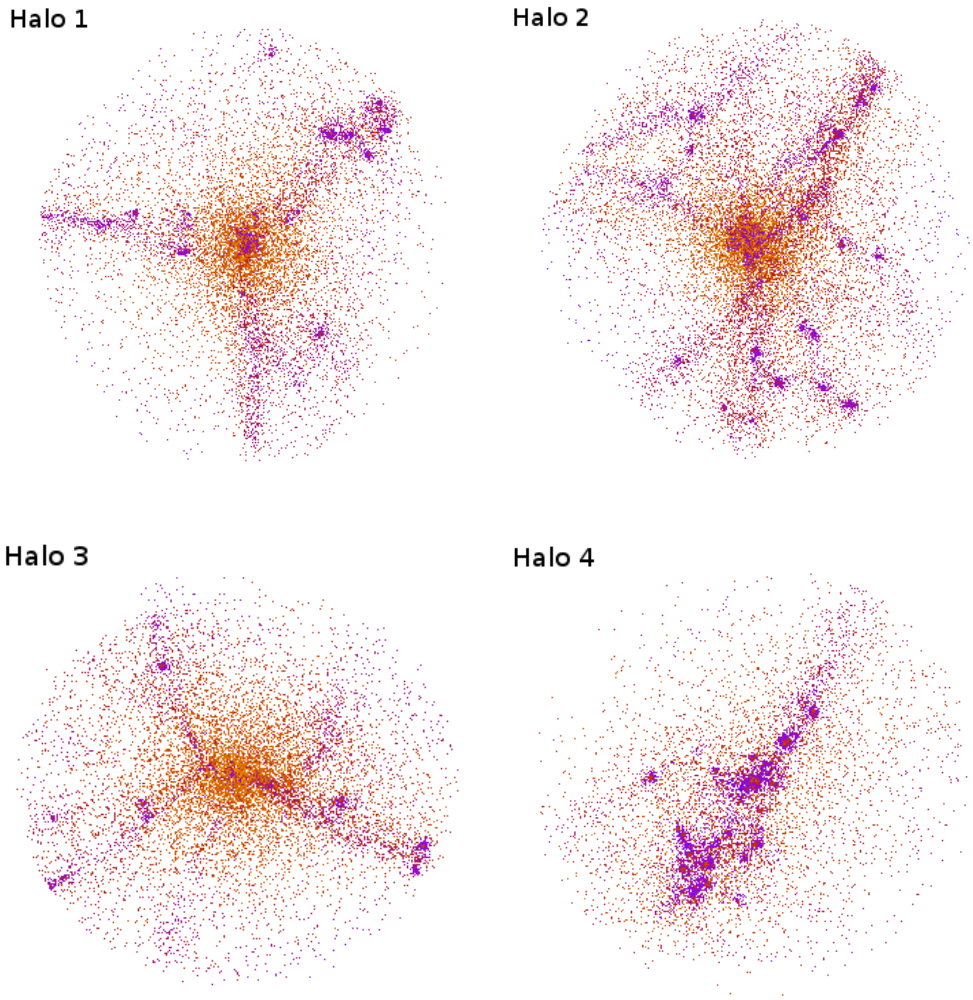

Fig. 3.1.: Portrait of the selected halos. Halo 1, 2 and 3 are in a range of -400 to 400 kpc for the space coordinates. Halo 4 is smaller and lies in a range between -250 and 250 kpc. The colors are a code for the temperature in Kelvin: $10^{2.5}$ is darkblue, $10^{4.5}$ is purple, 10^{5} is dark red, $10^{6.5}$ is orange.

within the cold flows. The streams of this halo do not lie in a plane.

Three of the five streams of Halo 3 show many small substructures. Two of the cold flows are narrow.

By looking at Halo 4 we can see that it has less hot gas than the other halos and that the cold clumps lie in a plane. The clumps in the halo center belong to the main galaxy and those incoming from the lower left belong to another gasrich galaxy that falls into the halo center. This infalling galaxy has a similar mass to the central object. Here a major merger event is taking place. We note that Halo

4 is less massive at this redshift. This halo was added because it has a beautiful disk at redshift 1.04 and we wanted to understand of there are connections between its disk at redshift 1.04 and the properties it has at higher redshifts. (For further details concerning the disk's properties see bachelor thesis of Felix Schulze.)

3.2. Properties at Redshift 2.33

To understand the nature of the cold flows and the halos in which they are penetrating, we investigate the distribution of the gas components and the dark matter, the pressure relations of the hot and the cold gas and compare the massflux to the starformation rate at z = 2.33.

3.2.1. Phase Diagram

To make the next steps more easy to follow we first want to show the phase diagram of the halo gas particles within three times the virial radius (R_{vir}). This radius will be taken most of the time because here the structure of the cold streams and even more the dark matter is (mostly) unmistakable. This will become important later when we trace the halos for different redshifts.

The diagrams show the different phases of the gas particles which will be specified as follows:

a) On the lower right side we find the particles that are heated by the shock with temperatures larger than 10^5 K and densities between 10^2 and $10^6 M_\odot/kpc^3$.

b) In the left middle with temperatures lower than 10^5 K are the particles for which the cooling processes (e.g. by metals) dominate the shock-heating of the surrounding medium.

c) At a density of about $10^6 M_\odot/kpc^3$ we see an edge at lower temperatures on the left side. These are the cold gas particles that are so dense, that they wander along this edge to higher temperatures to d).

d) The cold dense particles in c) become starforming multiphase particles, here seen as a continuous line in the upper right. The starforming multiphase particles in the simulation have formally a hot temperature component, in which the cold gas is embedded, but for our later calculations we will either treat them separatly or as cold gas particles, which depends on the features we want to study. A gas particle will become denser and hotter along this line and finally will form a star. We can

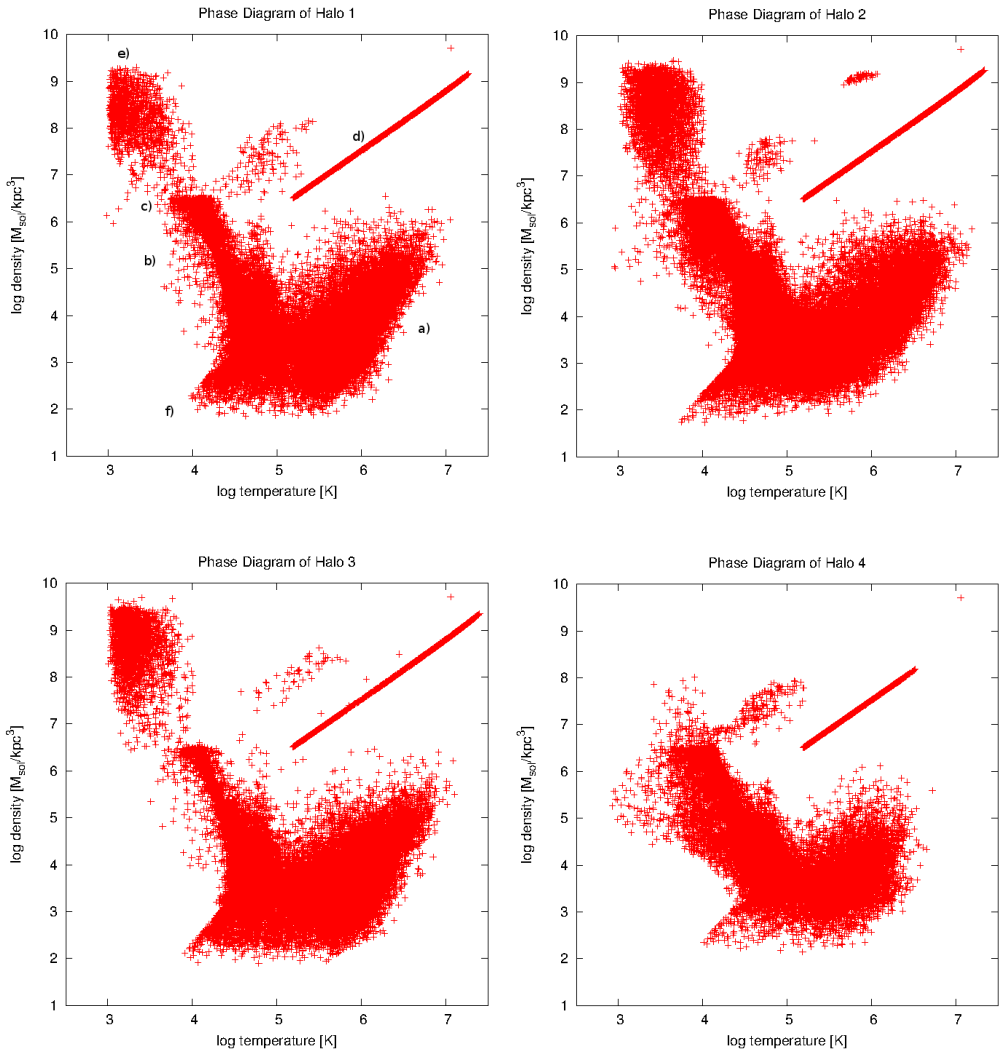

Fig. 3.2.: Phase diagrams of halos 1, 2, 3 and 4. In Halo 1 the different phases of the gas are marked: a) shock-heated gas particles, b) gas particles, where shock-heating is dominated by cooling, c) dense cold particles, which are about to form stars, d) starforming multiphase particles, e) gas particles, that have fallen back from the starformation, f) adiabatic tail

also see that the particles on this branch are in equilibrium where the temperature is proportional to the density.

e) As described earlier one gas particle can form four stars. After one starforming particle has formed one star the rest of the particle either goes on forming stars or falls back to the upper left, where the density is very high and the temperature low or in some cases fall back to the shock-heated particles with higher densities (b)).

f) In the lower left we see the adiabatic tail, which is only interesting if the

filaments of the cosmic web are investigated.

By comparison of these four diagrams we can see that Halo 1 and 3 are very similar. Halo 2 has a lot of hot gas and many stars seem to have formed due to the number of gas particles that have already formed stars in the upper left. The least massive Halo 4 has generally less gas particles and the gas has not been heated over 10^7 K yet. The branch of the starforming particles is not as long as in the phase diagrams of the other halos. Most interesting, the star formation has not been turned on yet, which we conclude from the fact that there are almost no gas particles that have already formed stars in the upper left.

An important fact that we learn from this phase diagram is that we will have to cut the temperature at 10^5 K for making further investigations for the different behavior of the cold and the hot gas. So for some calculations (e.g. mass flux) we have to count the hot multiphase particles to the cold gas due to the fact that, as we will see in the next section, these starforming multiphase particles are embedded in cold clumps within the cold streams.

3.2.2. Distribution of the Different Components

The next thing we want to explore is how the different types of particles are distributed within $3R_{vir}$.

In Fig. 3.3 we show the plots for Halo 1, where one thing is particularly striking: The cold gas seems to follow the dark matter distribution. It is what we have expected, since the dark halos of the galaxies are embedded in the filaments of the cosmic web. As described earlier these filaments consist of dark matter and cold gas which condensates in the dark matter troughs to form galaxies. Another aspect we see in the lower left panel is that the cold gas distribution shows a filament-like structure, whereas the hot gas is spherically symmetric spread around the halo center, which matches the investigations of Dekel and Birnboim (2006). In the cold streams we find some substructures or cold clumps where the density is so high that the gas particles begin to form stars (turquoise stars in Fig. 3.3). We also see that most of the stars are in the central halo. At this point we could ask the question whether stars form in these clumps before they reach the halo center. We will come back to this question later, when we discuss the evolution of the halos.

The plots for the other three halos are added to the Appendix but we briefly want to describe the special features of each of them.

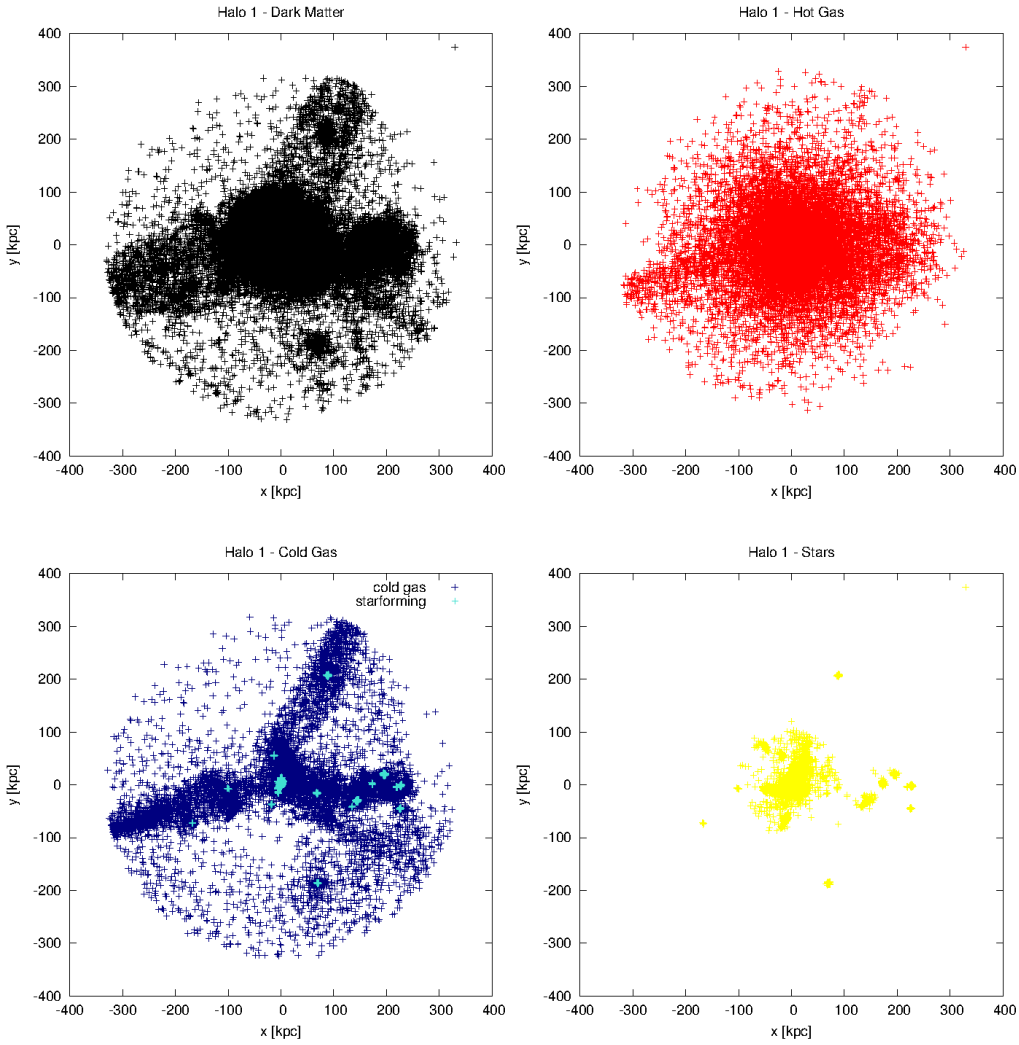

Fig. 3.3.: Components of Halo 1 in $3R_{vir}$ projected onto the xy-plane: upper left: dark matter, upper right: hot gas, lower left: cold gas incl. starforming multiphaseparticles, lower right: stars

Two of the cold gas streams of Halo 2 (Fig. B.1) seem to be surrounded by hot gas and we see some small infalling star clusters along these two streams.

Halo 3 (Fig. B.2) shows an elongated star-region in the center, which could be the result of a merger. This idea is supported by the dark matter distribution because it is not spherically symmetric in the center but elongated.

Halo 4 (Fig. B.3) shows two seperate structures, especially in the distribution of the stars, but also in the cold gas and the dark matter distribution.

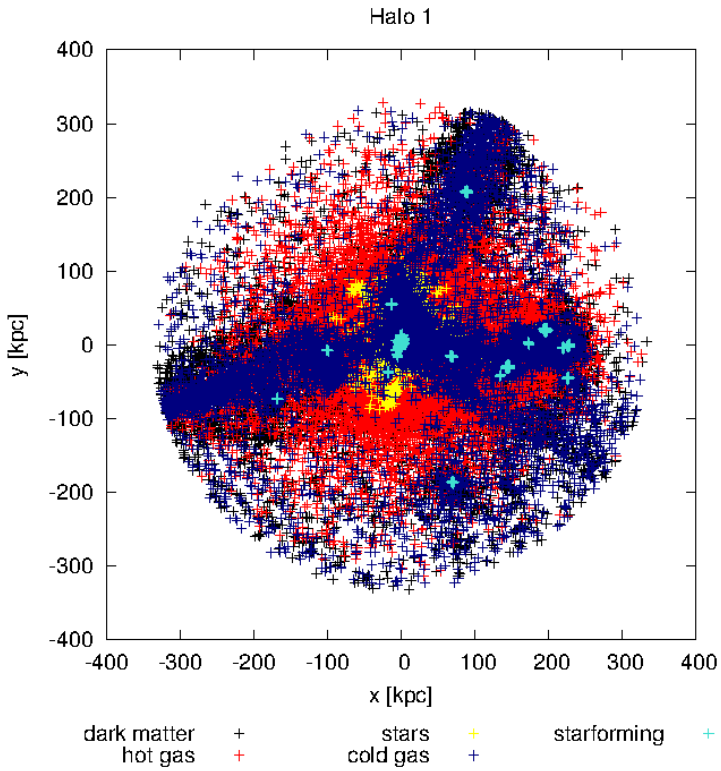

Fig. 3.4.: All components of Halo 1 in $3R_{vir}$ projected onto the xy-plane, colors: black is dark matter, red is hot gas, stars are yellow, navy is cold gas and turquoise are starforming particles

3.2.3. Pressure and Density in the Halos

To address the question whether the hot and the cold gas are in equilibrium, we will calculate the pressure and density of these two components. Fig. 3.5 shows the density times internal energy for the hot gas (upper left), the cold gas (upper right) and the starforming particles (lower panel) separately against the radius for Halo 1.

First we want to see how the hot gas behaves relating to the pressure: Between $3R_{vir}$ and R_{vir} the pressure is between 10^{-14} and 10^{-11} Pa with the lower edge rising in direction to R_{vir}. From R_{vir} to the center the pressure increases. This is due to the fact that the pressure has to compensate for the gravitational force, which is increasing towards the halo center.

The shape of the curve for the cold gas is almost the same between $3R_{vir}$ and R_{vir} as for the hot gas, but the cold gas shows peaks. These peaks are related to substructures that have a higher pressure due to the higher density (as we will see later).

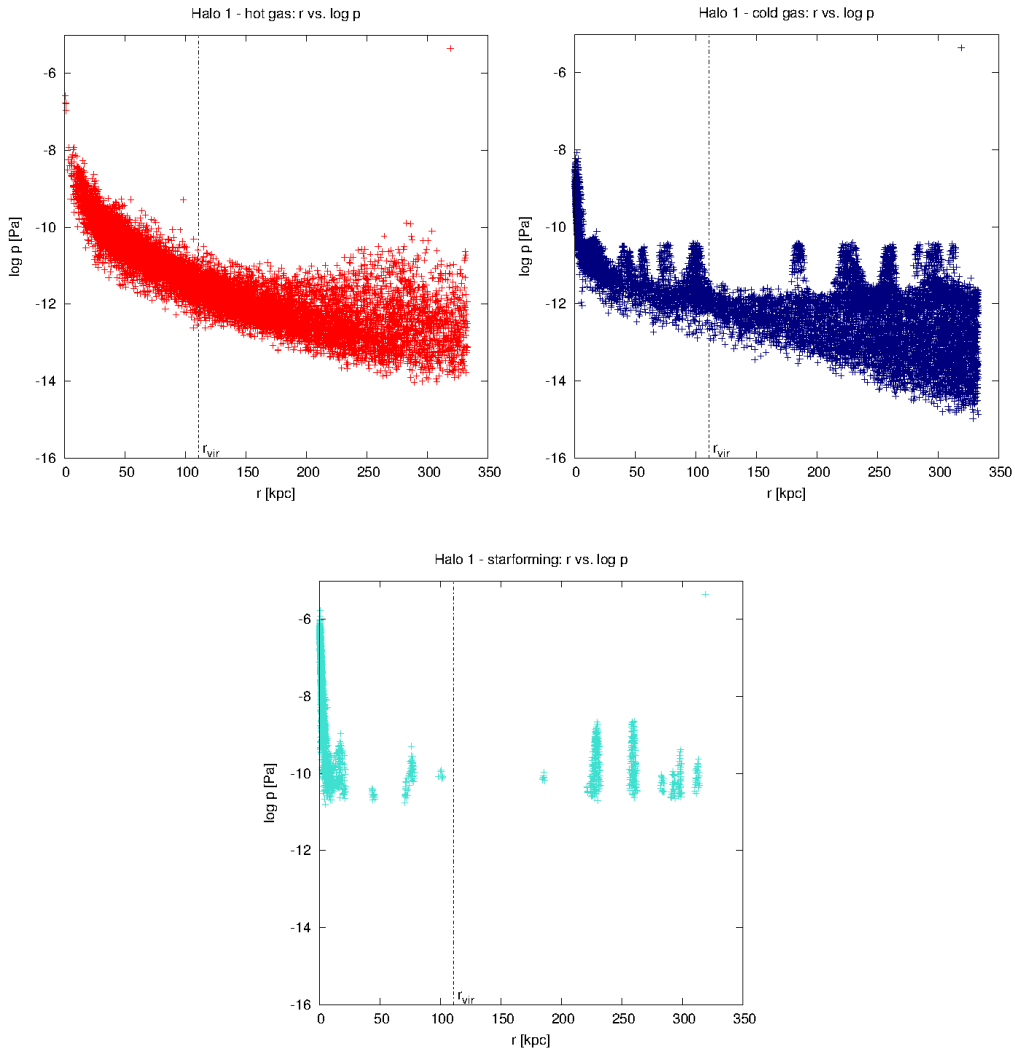

Fig. 3.5.: Radius vs. pressure-diagram of Halo 1 within $3R_{vir}$. Upper left: Hot gas, upper right: Cold gas, lower panel: Starforming particles

Due to the self-gravity the pressure of the multiphase particles in those clumps of cold gas is very high and thus they begin to form stars. We also see that the main activity of star formation takes place in the center of the halo. By comparing the cold and the hot gas it seems like these two components are in pressure-equilibrium because no significant difference in pressure is visible for the range between R_{vir} and $3R_{vir}$.

By comparing the pressure diagrams for the halos (see Fig. 3.6) we note that the pressure of the hot gas in Halo 2 is very high near the center and that there is also a gathering of cold clumps that are about to form stars within R_{vir} (upper right

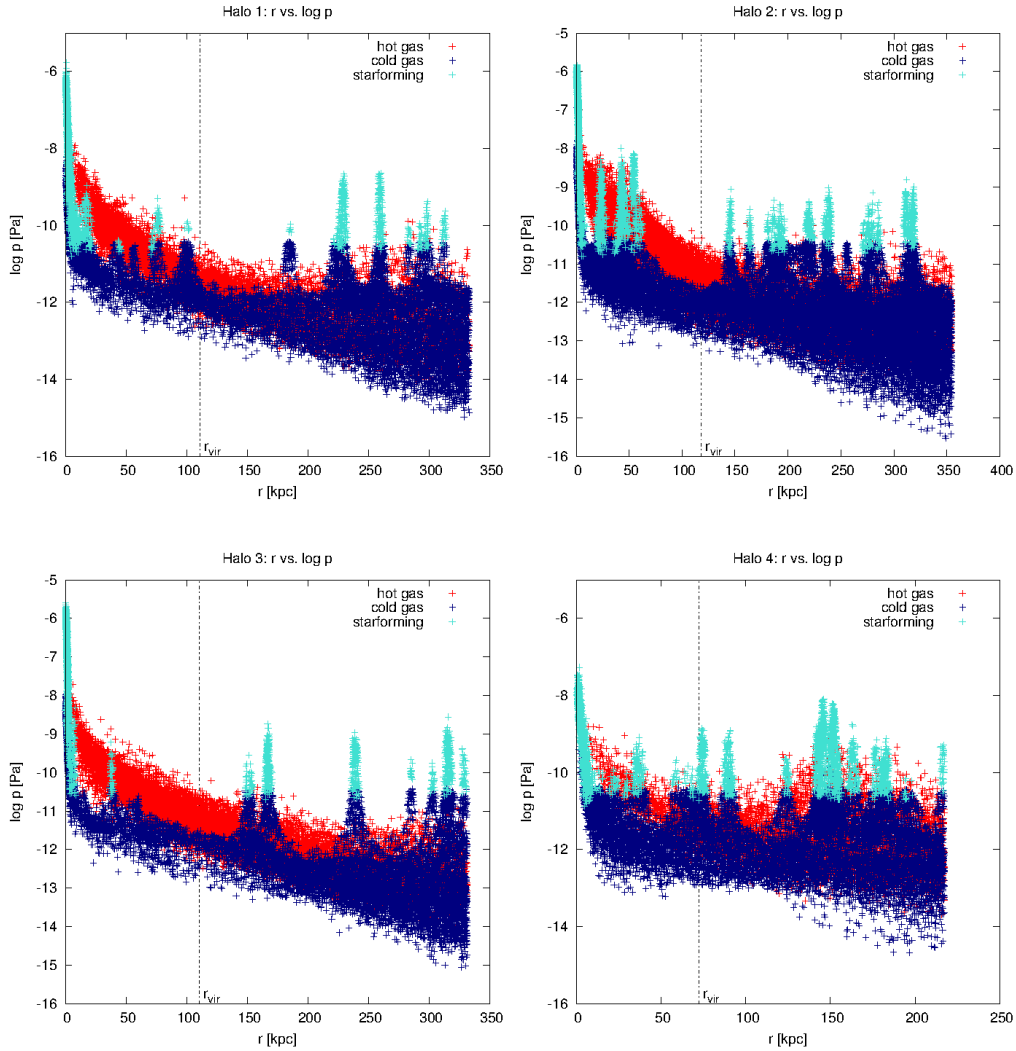

Fig. 3.6.: Radius vs. pressure for all halos. Hot gas is red, cold gas is navy and starforming particle sare turquoise. The pressure of halos 1, 2 and 3 increases within the virial radius to compensate the growing gravitational force. Halo 4 has a cumulation of substructures, which is a strong indication for a merger.

panel).

The hot gas of Halo 4 does not have such a high pressure like the other halos and it has two maxima: one near the center and the other at about 150 kpc. Even more important , we can also find a clustering of cold gas substructures at 150 kpc, which have as high pressure as the starforming particles in the center of the halo. This is a possible indicator for a merger that is going to happen.

The pressure relations become clearer by looking at Fig. 3.7 where density is plotted against radius, also separately for the cold, hot and starforming particles for Halo 1 and Fig. 3.8, where all components in one plot are shown for halos 2, 3 and 4.

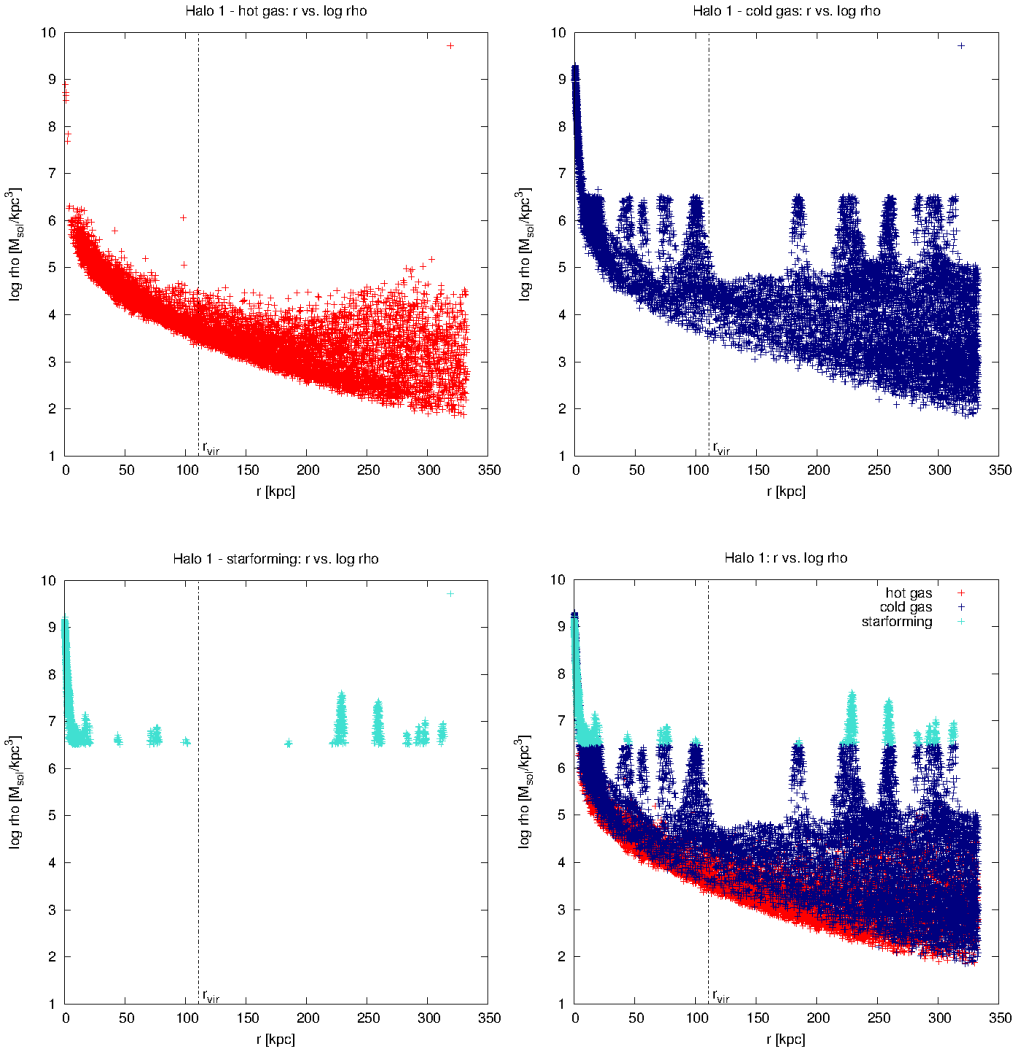

Fig. 3.7.: Radius vs. density diagrams of Halo 1 for the single components: hot gas is red, cold gas is navy and multiphase particles are turquoise

In general the density of the hot gas is a little lower than that of the cold gas. It increases on the hot gases position to the center of the halo because, as we have seen in the radius vs. pressure diagram, the pressure is high at the center and proportional to the density. The cold gas has a higher density than the hot gas and the substructures are eye-catching, since their high densities stand out. Here again the very dense starforming particles can be found on top of the cold gas

substructures.

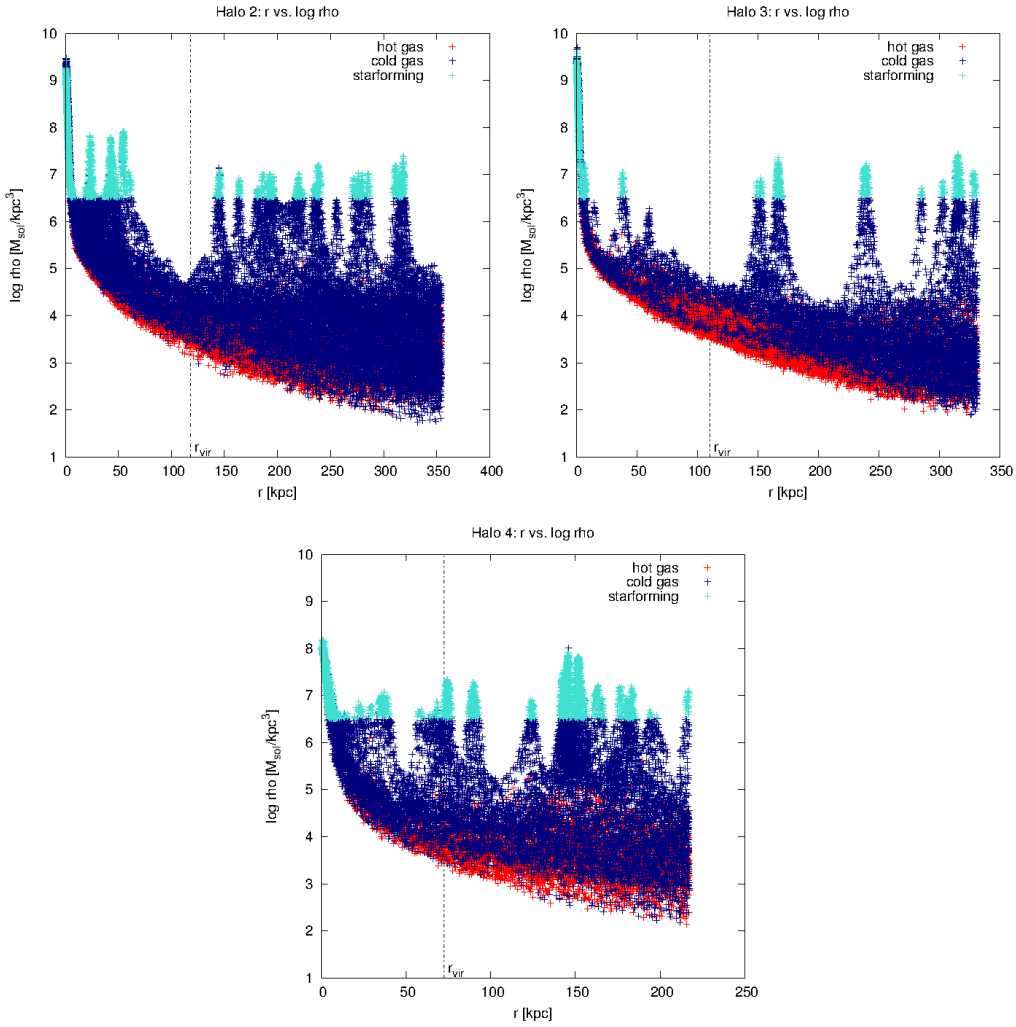

Fig. 3.8.: Diagrams of the halos 2, 3 and 4: radius vs. density. Hot gas is red, cold gas is navy and starforming particles are turquoise

Halo 3 only has few substructures, whereas Halo 2 and 4 have many substructures, similar to Halo 1. We see that Halo 4 has a density that is slightly higher than that of the other halos and at about 150 kpc there is a cumulation of substructures, as seen before, and the hot gas has a higher pressure, which could imply a merger. We also note that the density in the center of Halo 4 is not significantly higher than in the substructures. Together with the phase diagram this confirms the picture of a young halo that has not been forming many stars yet.

3.2.4. Radial Velocity of the Inflowing Gas

We investigate the radial velocity of the hot gas and the cold gas including the multiphase particles to understand whether the particles flow in with a constant velocity or whether the velocity changes along the streams. We select particles with a negative radial velocity because we are interested in particles heading towards the halo center.

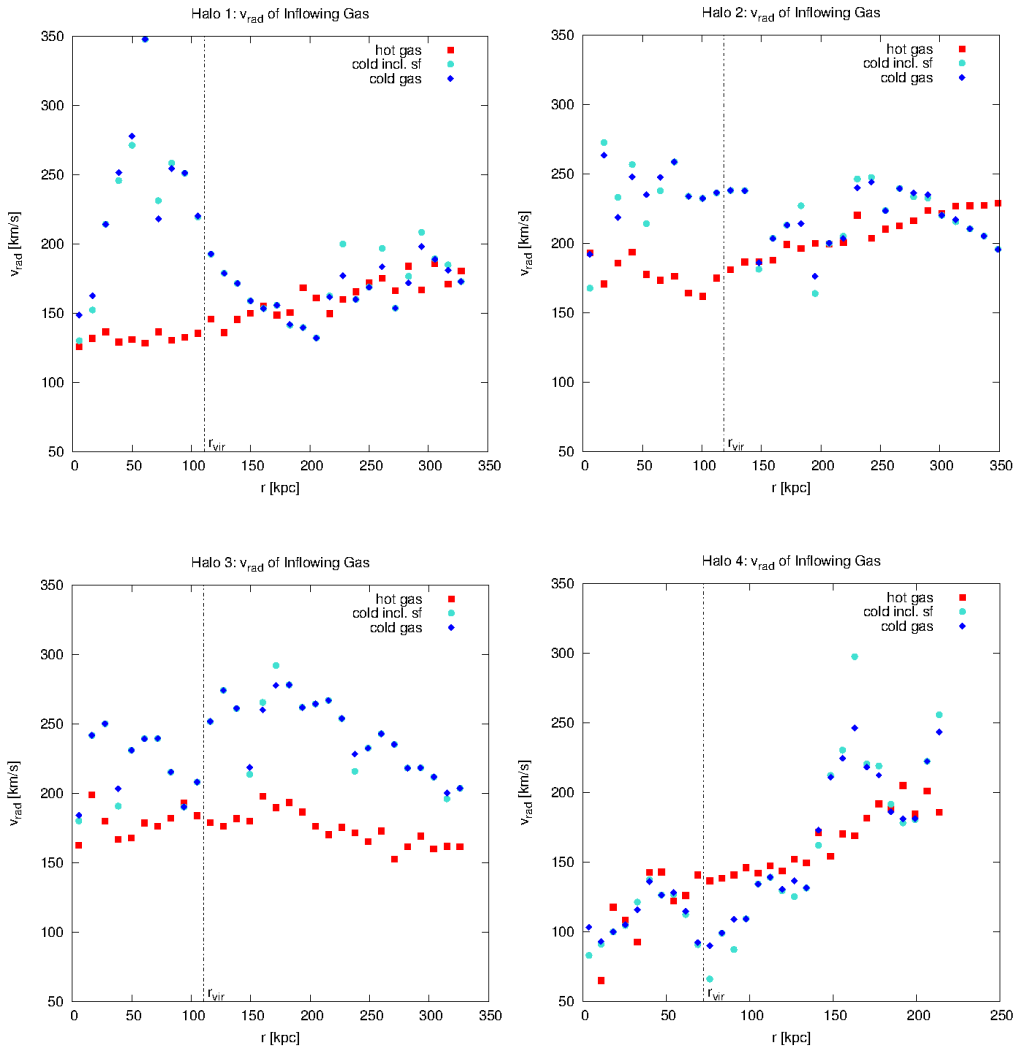

Fig. 3.9.: Radius vs. radial velocity of the gas particles streaming inward

We find that the radial velocity of the hot gas in Halo 1, 2 and 3 is almost constant with radius. As seen in Fig. 3.9, only Halo 4 shows a different picture: From the hot gas entering $3R_{vir}$ to the halo center the radial velocity drops about 200 km/s.

The cold gas does not seem to have an obvious pattern. Halo 2 and 3 have relatively constant radial velocities, which matches the assumptions by Dekel et al. (2009a). The radial velocity of the cold gas in Halo 1 increases up to half the virial radius, which could be interpreted as a free fall from the gas. From 0.5 R_{vir} to the center a linear decrease of the radial velocity follows. Halo 4, here again, shows a peak in the radial velocity at 150 kpc, where the massive substructure is. This can be explained by the fact that this substructure has its own rotational velocity, which adds to the velocity of the main halo.

(Note: The first bin from the center outwards has no entry because there are no hot particles in this bin that flow inwards.)

3.2.5. Massflux

The massflux is the key to understanding starformation in galaxies and the evolution of the halos, since it is directly proportional to the starforming rate, as mentioned in the theoretical foundations. In the left panel of Fig. 3.10 we see the massflux of the hot gas component for Halo 1 within $3R_{vir}$ split in inflowing, outflowing and net massflux. Due to the turbulence of the hot gas, almost as much hot mass is flowing in as is streaming out, which results in a net massflux around 0 (within R_{vir}) and 50 $M_{\odot}$/yr ouside R_{vir}.

The right plot shows the massflux of the cold gas. We want to note that in the following discussion 'cold' refers to cold gas inclusive the multiphase particles. Here we can see clearly that the outwards massflux is nearly zero. Only at the halo center there seems to be a turbulence, which affects also the cold gas. There are some peaks in the net and inflowing massflux, that are related to substructures. We will take a closer look to that a little later.

By comparing the net massfluxes of the four halos in Fig. 3.11 we can see that the hot massflux is constant between 0 and 50 $M_{\odot}$/yr for all halos. The massflux of Halo 2 and 4 is slightly increasing with radius.

The cold mass flow rates are higher than the hot ones and not constant within $3R_{vir}$. They have some peaks at the radii of the substructures. Halo 1 has a peak between 220 and 250 kpc. The massflux of Halo 2 is higher than the massflux of the other halos and the massflux is higher in the regions, where the substructures are (between 150 and 350 kpc). The diagram for Halo 3 also shows peaks at the positions of the substructures (at about 150 kpc, 250 kpc and 300 kpc). A significant peak at about 150 kpc is seen in the mass flow rate of Halo 4. Here the massflux

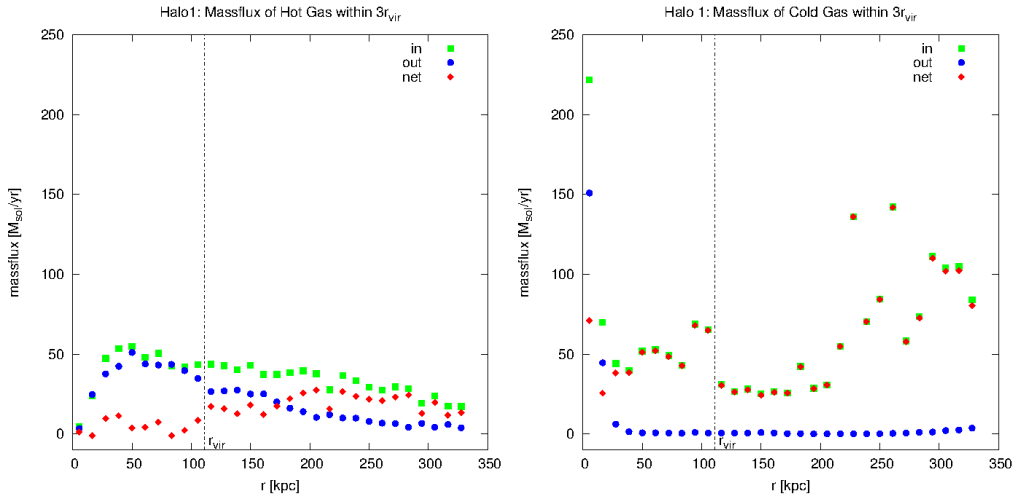

Fig. 3.10.: Radius vs. Massflux for hot (left) and cold incl. multiphase particles (right)

is about 350 $M_\odot$/yr, which indicates that there must be a very large substructure flowing in.

In Fig. 3.12 we show the massflux within the virial radius for the four halos. We can see that the massflux is constant for the Halos 1, 3 and 4. The massflux of Halo 2 increases in direction to the center of the halo. At about 45 kpc we see a cold outlfow, which could be the result of the interaction between the main galaxy and a large substructure.

We also see a hot massflux outwards. To see if this has any correlations with the accretionrate of the AGN, we compare the ratio of the accretion rate of the black holes in the center of Halo 1, 2 and 3 with the Eddington accretion rate, which is the maximum accretion rate of a black hole. We find that the ratio of the main BH in Halo 2 is $4{\cdot}10^{-2}$, for Halo 1 it is $8{\cdot}10^{-6}$ and for Halo 3 we get $7{\cdot}10^{-4}$. This indicates that there is a strong AGN feedback in Halo 2, which throws out hot gas and thus the hot massflux is negative at half the virial radius.

We compare the pressure relations with the massflux of the single halos to see if there are connections between these two properties.

In Fig. 3.13 we can see that the massflux of the cold gas correlates with the peaks of the pressure of the cold and starforming particles. Where the pressure is high, there are substructures that are moving inwards.

Halo 3 has relatively high cold massflux between 175 kpc and 275 kpc (compared

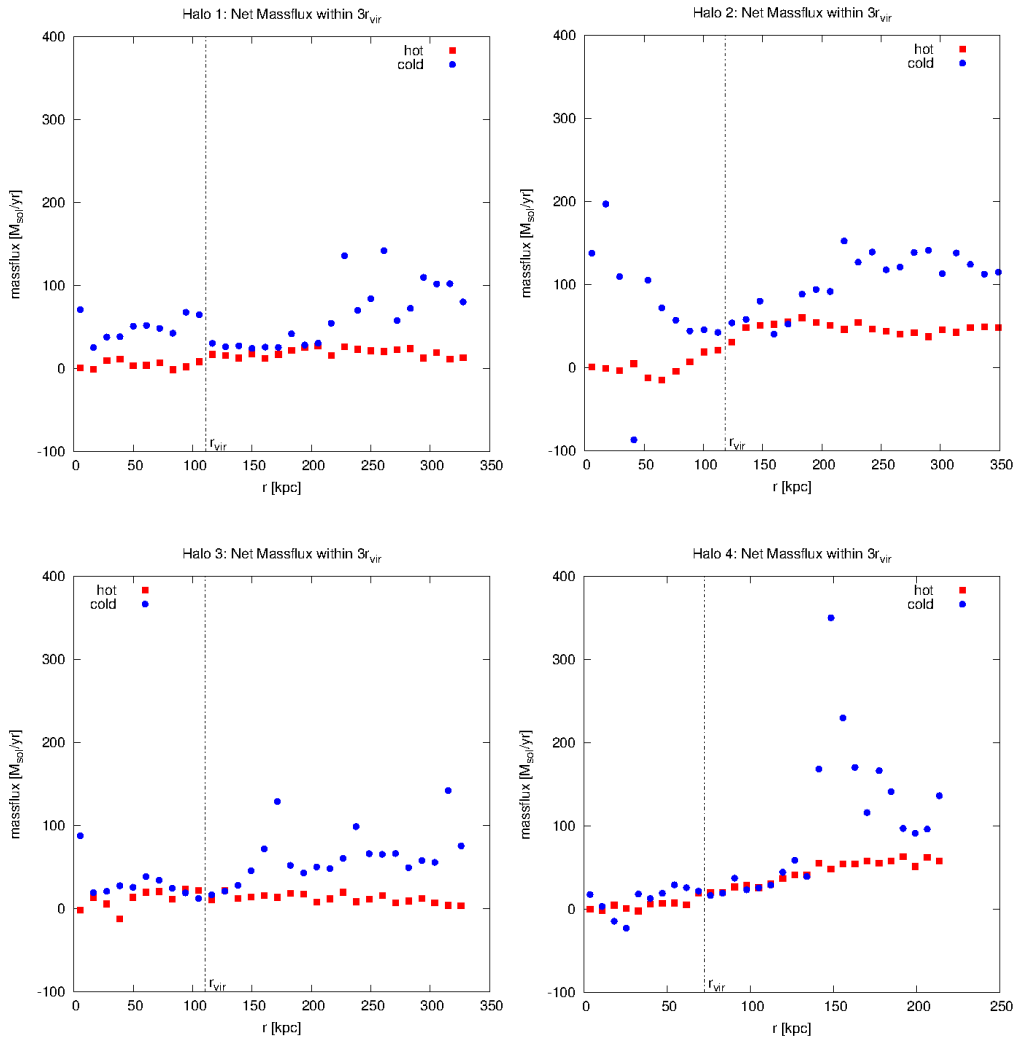

Fig. 3.11.: Radius vs. net massflux for halos 1, 2, 3 and 4. Cold particles include the starforming ones within $3R_{vir}$

to the massflux along the radius) although there are no substructures besides one peak at 230 kpc. This could be mass flowing in along a smooth cold stream.

The massflow rate of Halo 4 is generally very high, so we have to take a closer look to find indications of a correlation between the pressure and the massflux within R_{vir}.

3.2.6. Mean Temperature along Cold Stream

We now want to see how the temperature of the cold gas in the flows varies between $3R_{vir}$ and the halo center. Therefore we selected the particles with a temperature

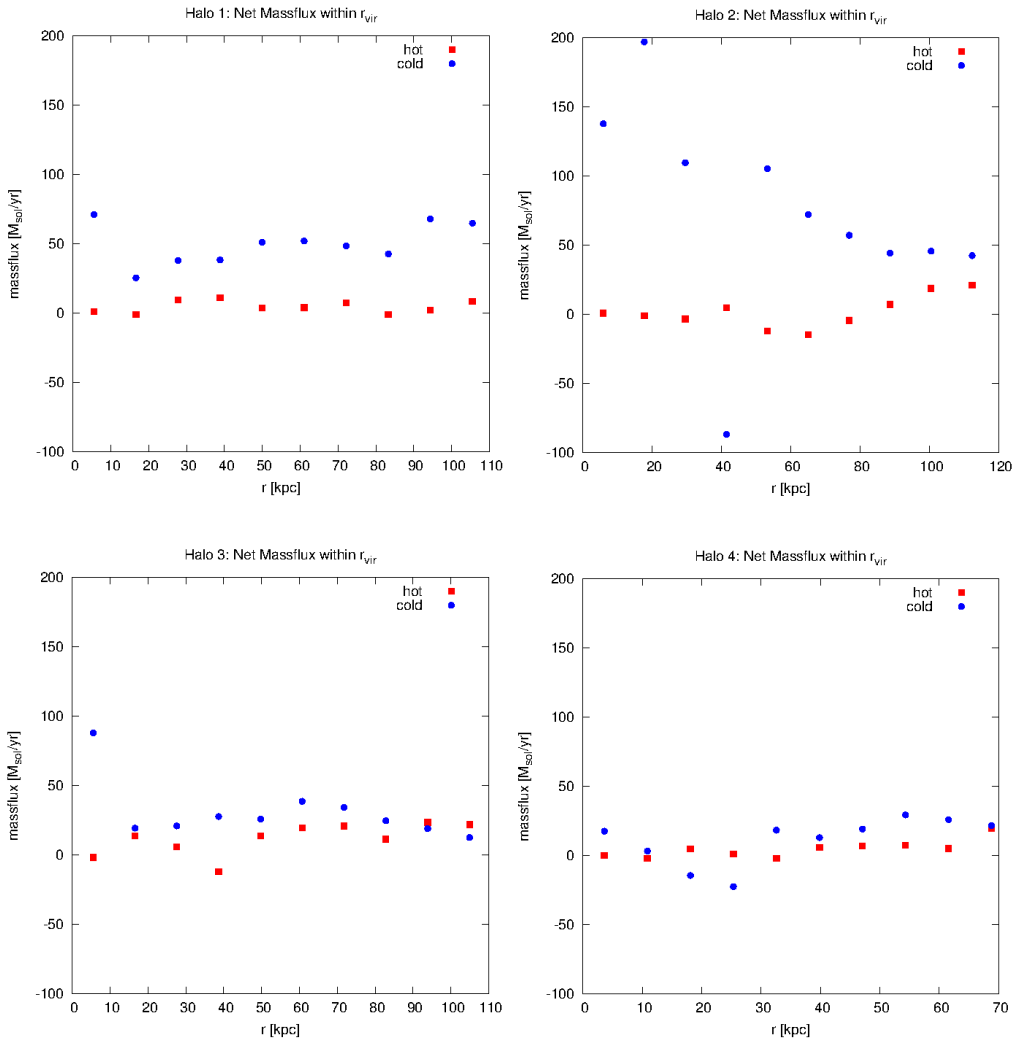

Fig. 3.12.: Radius vs. net massflux for halos 1, 2, 3 and 4. Cold particles include the starforming ones within the R_{vir}

lower than 10^5 K and a radial velocity in direction towards the center. To see a relation between the temperature and the star formation rate we added the behavior of the cold gas particles including the starforming ones, which is plotted in Fig. 3.14.

In general the temperature between $3R_{vir}$ and R_{vir} is constant. For smaller radii than R_{vir} the temperature drops along the stream towards the halo center. Furthermore, the temperature drops exactly at the positions where the temperature for the cold gas including the starforming particles is higher than the average, i.e. where substructures are. This is due to the high density of the cold gas. The cold gas is so dense that self-gravity dominates and the cold and ever denser gas begins to form

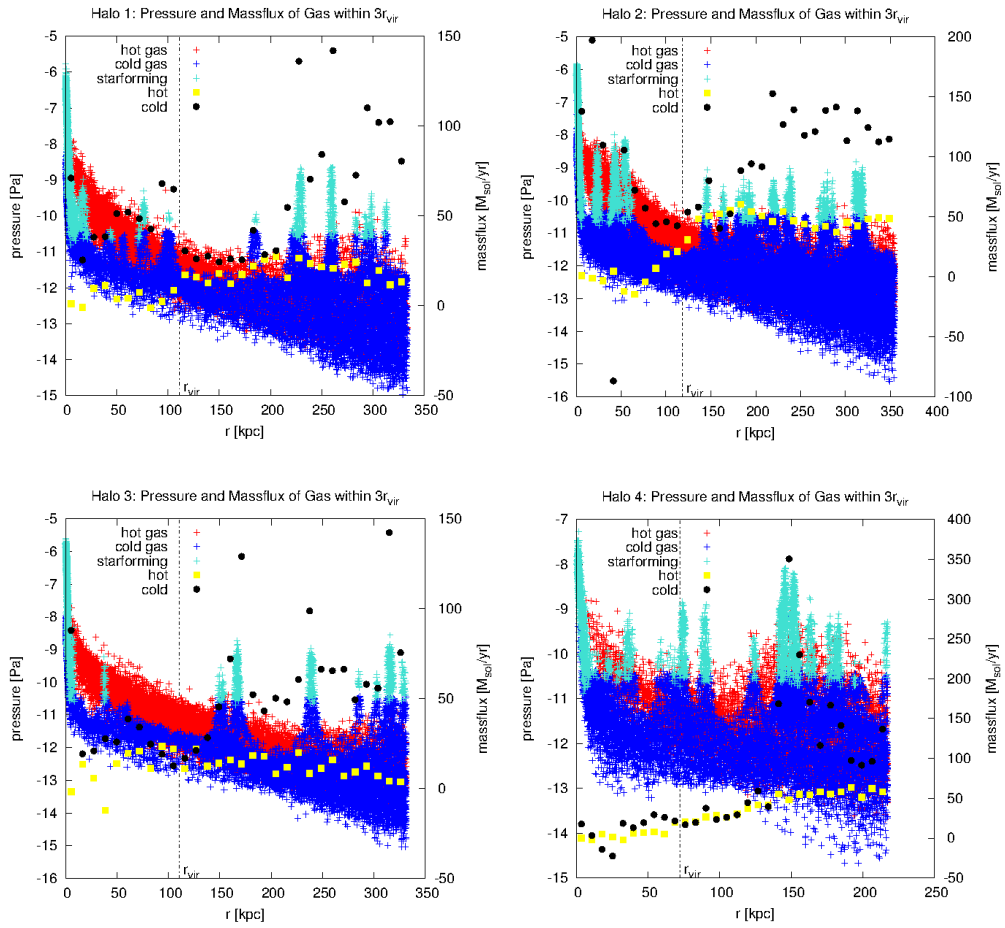

Fig. 3.13.: Radius vs. pressure on the left scale and on the right scale massflux cold(incl. starforming) and hot for Halos 1, 2, 3 and 4.

stars.

The cold gas of Halo 1 is relatively constant at $10^{4.6}$ K and then drops at about 25 kpc to $10^{3.9}$ K near the center. Halo 2 has also a constant temperature of about $10^{4.6}$ K but is dropping earlier than Halo 1, namely from R_{vir} inwards. Halo 3 shows a similar behavior, after it slightly increases from $3R_{vir}$, where it enters with $10^{4.55}$ K and reaches $10^{4.8}$ K.

In the diagram for Halo 4 we can again see the substructures. We expected a deeper drop in the temperature of the cold gas and a higher one of the cold gas inclusive the starforming particles. The explanation might be the rotation of the small clumps around their own center, i.e. the substructures do not all have a velocity pointing towards the halo center of the host galaxy.

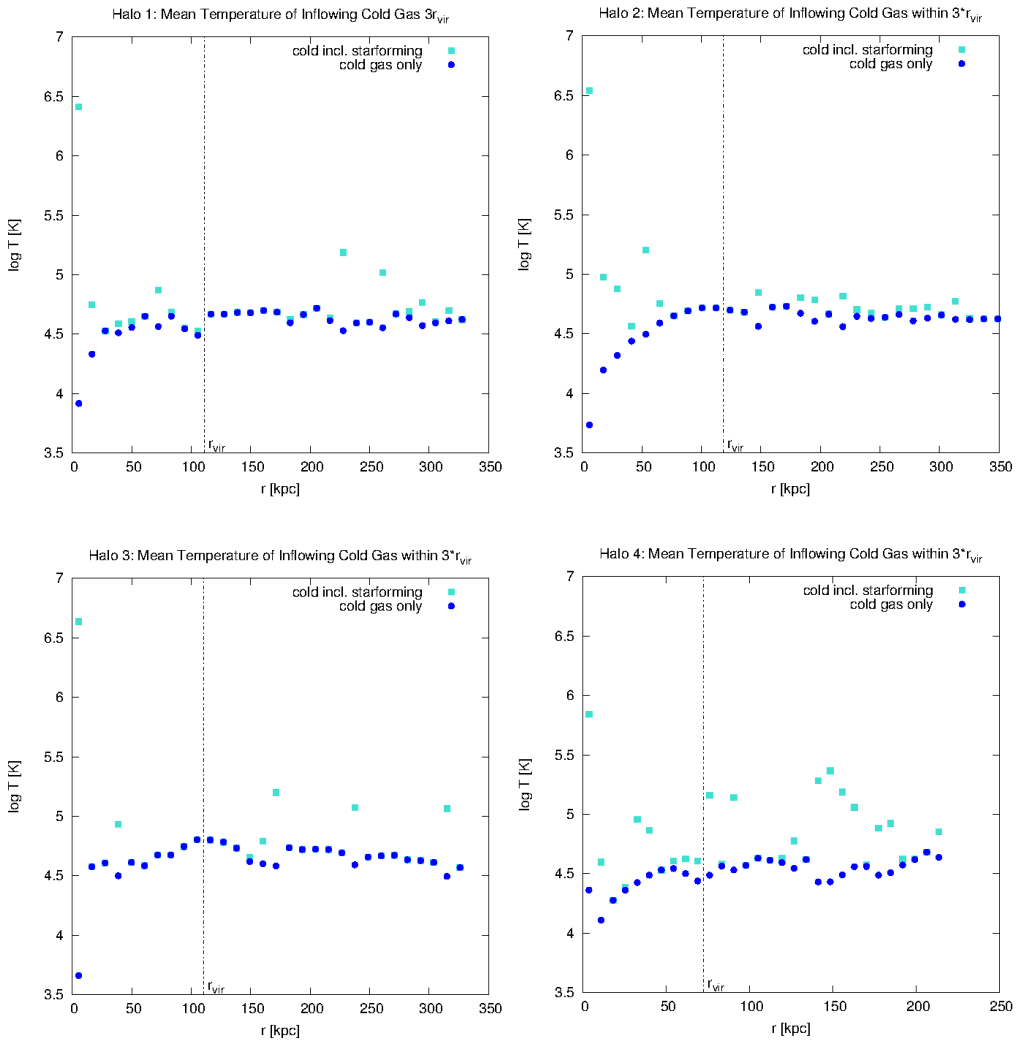

Fig. 3.14.: Mean temperature of the cold particles and the cold particles including the multiphase particles along the streams inwards.

We now want to understand if the mean temperature is representative for all the cold gas particles. Therefore we study the distribution of the number of incoming gas particles in a temperature interval between 10^4 and 10^5 K (see Fig. 3.15).

Halo 1 has its maximum in the given temperature range at about $3 \cdot 10^4$ K with 1600 gas particles. By regarding the plot for Halo 2 we see (approximately) a plateau between $3.5 \cdot 10^4$ and 10^4 K with about 2100 particles, i.e. Halo 2 has many cold particles. Maybe the maximum number of gas particles is not reached yet and lies at even lower temperatures than investigated. Halo 3 has its maximum at $3 \cdot 10^4$ K and with about 1100 particles not as many as the other three halos. In the diagram

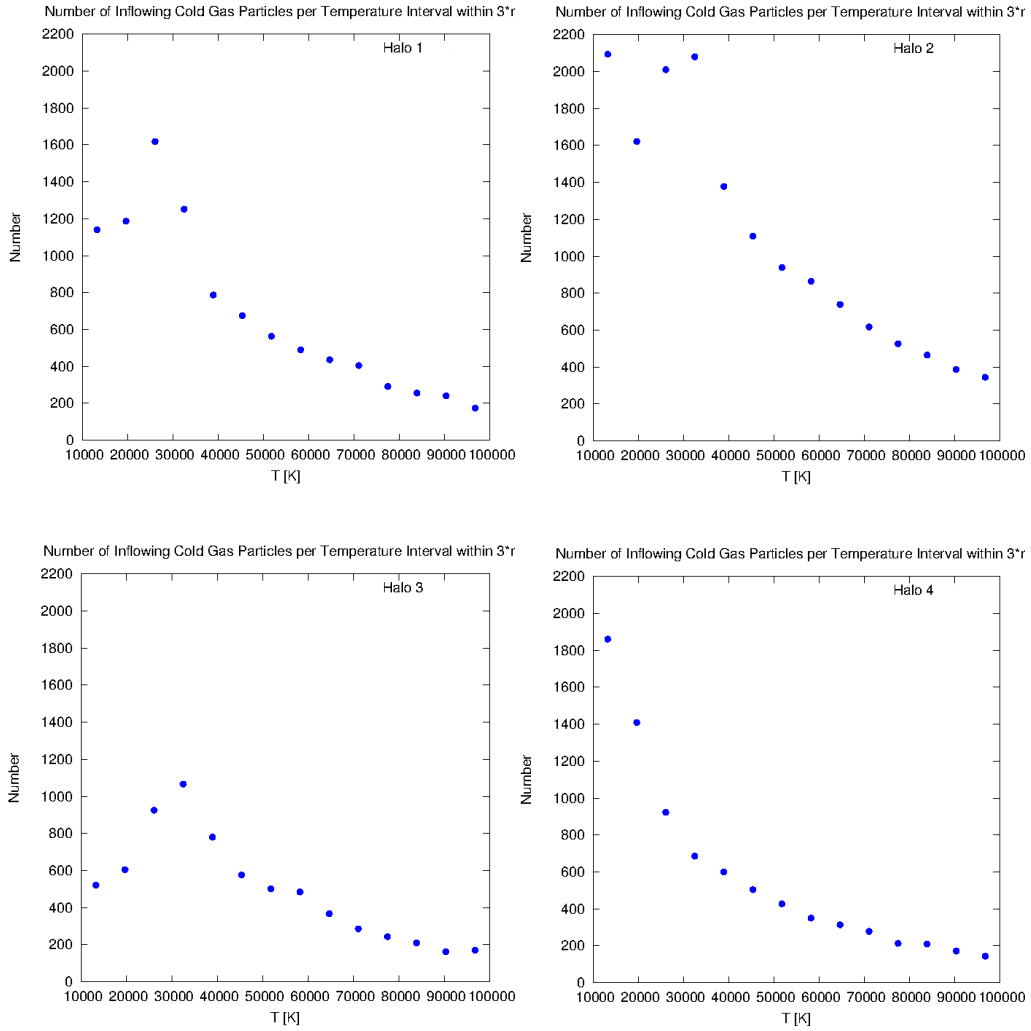

Fig. 3.15.: Number of particles streaming inwards with a temperature in the range 10^4 and 10^5K within $3R_{vir}$. The interval is parted into 14 tics.

for Halo 4 we see a maximum at 10^4 K with 1900 gas particles. But we strongly assume that the maximum of the particle number is not reached yet. This halo has probably more even colder gas below the lower temperture limit of the studied interval.

We conclude that the mean temperature of the cold gas moving inwards is representative for the cold stream if we take account of the cold gas particles that gather in clumps and are about to form stars. They contribute more to the mean temperature than the smooth part of the cold flows. Hence the number of particles

in the selected interval has its maximum on the left side.

3.2.7. Starformation Rate

In the following subsection we study the starformation rates of the Halos 1 and 4. Halo 1 was chosen as an example for a halo which has cold smooth streams, Halo 4 as an example for a merger situation. We want to see how the starformation along the radius is distributed and if they are related to the massflux. In Fig. 3.16 every symbol shows the starformation rate within one of the 14 bins within $3R_{vir}$. (We have not plotted the same range for Halo 1 and 4 because we do not want to compare the two halos but the relation between the massflux and the SFR in the selected halo.)

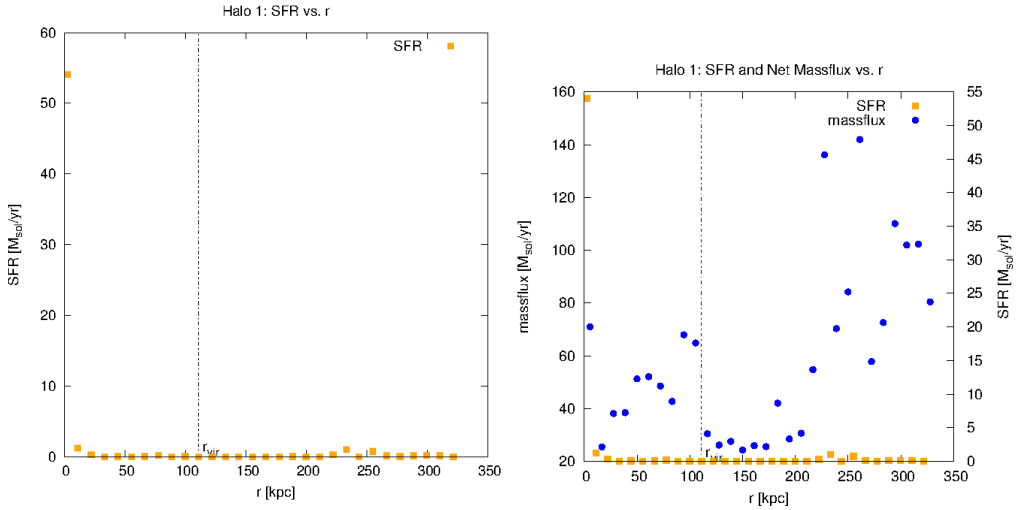

Fig. 3.16.: Halo 1: Left: The starformation rate within the 14 bins. Right: The SFR (right y-axis) compared to the massflux of the cold gas incl. multiphaseparticles(left y-axis).

By looking at Fig. 3.16, showing the results for Halo 1, we can clearly see that the main starformation takes place in the halo center within 5 kpc. Besides that, almost no stars are formed outside a range of about 16 kpc. How does that fit to the massflux of the cold gas which is very high at e.g. 230 kpc? The starformation rate of about 1 $M_{\odot}$/yr outside 16 kpc indicates that there is a massflux of smooth gas particles and gas clumps that will reach the center before they evolve into stars.

As expected, Halo 4 shows a different picture, as can be seen in Fig. 3.17. Here the starformation rate at the center is about 10 $M_{\odot}$/yr, which means that this halo is very young and a starburst is happening. The most interesting thing is that there

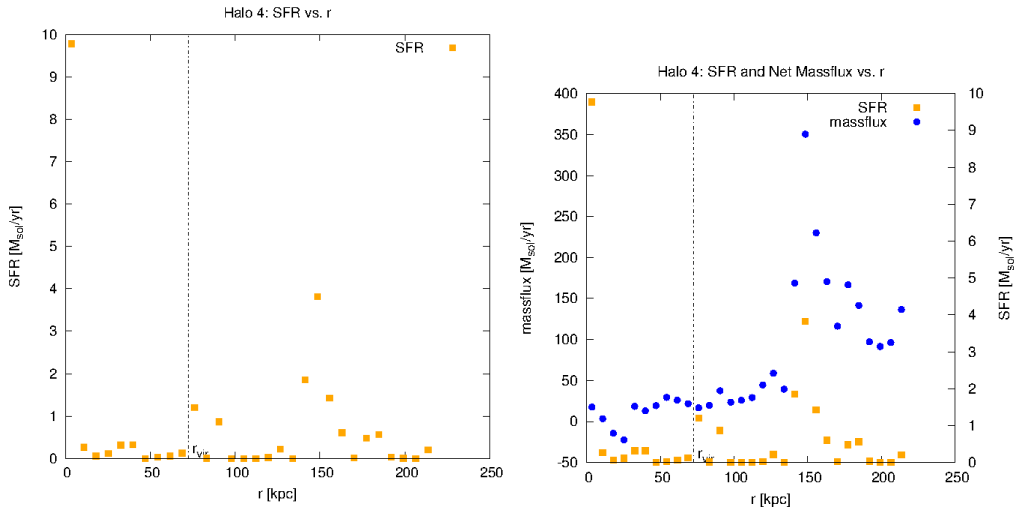

Fig. 3.17.: Halo 4: Left: The starformation rate within the 14 bins. Right: The SFR (right y-axis) compared to the massflux of the cold gas incl. multiphaseparticles(left y-axis).

are peaks in the starformation rate where the large substructure falls in, i.e. the substructure also has a starburst. This matches the merger scenario.

Concluding we can say that the starformation rate of Halo 1 is representative for a halo that has no major mergers and Halo 4 shows how the starformation rate is distributed for a halo which undergoes a merger.

3.2.8. Subhalos

The last thing we want to study in this section are the properties of the substructures, especially the mass relations within the subhalos.

We will have a closer look at the substructures of Halo 1. (Note: For the investigation of the properties we have excluded the central halo.)

In Fig. 3.18 we see the distribution of the 25 subhalos in yellow and the cold gas in blue. Most of the subhalos are within the cold streams or embedded in clumps of cold gas. There is one stream in the upper right, along which only one subhalo falls in. In contrast on the lower right we see a cold flow with many substructures on their way towards the halo center.

For the investigation of the mass relations we have plotted the logarithmic mass of the dark matter versus the logarithmic mass of the gas (see left side of Fig. 3.19). Every point in the plot represents a subhalo. We can see that there is a linear correlation between the mass of the dark matter and the mass of the gas in the

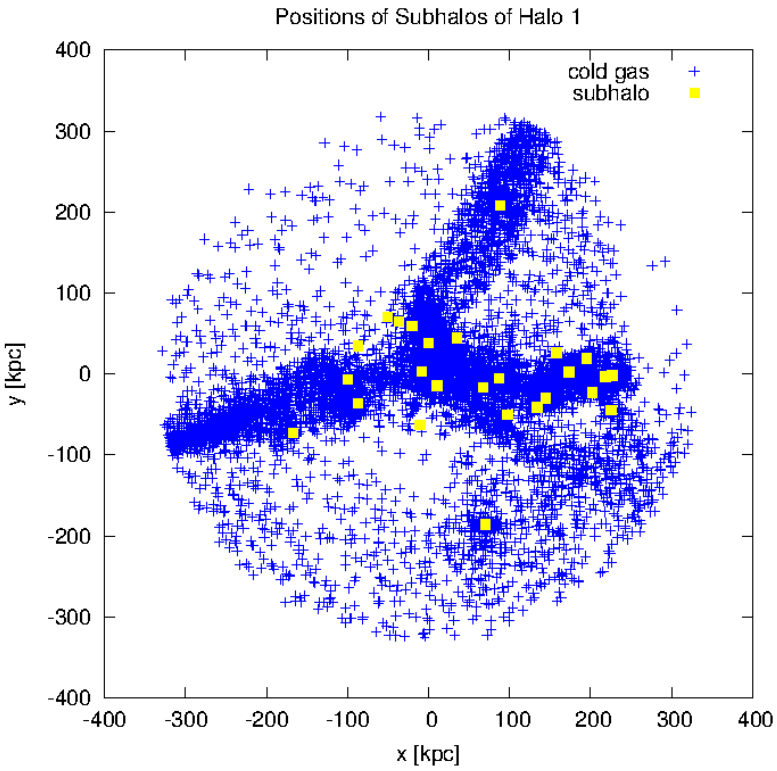

Fig. 3.18.: Halo 1: The positions of the subhalos (yellow) in the xy-plane. The cold gas partilces are blue.

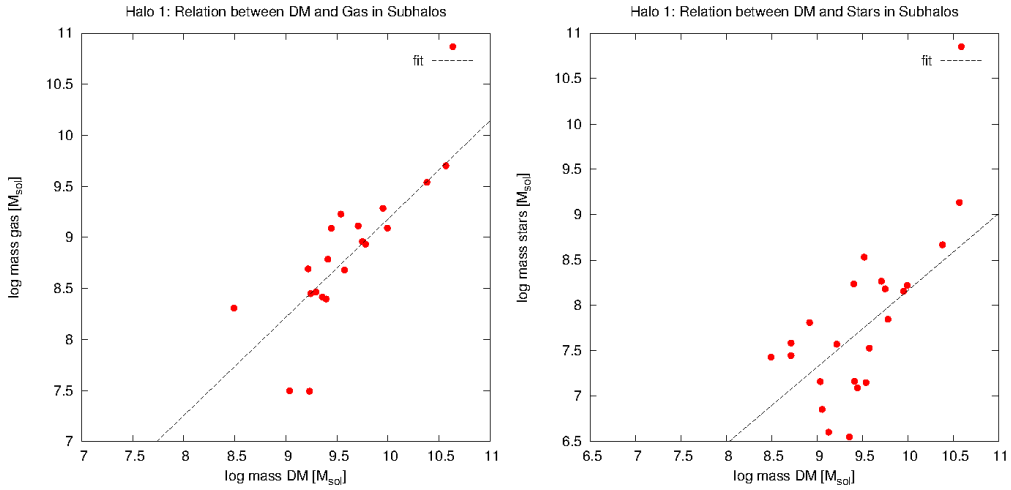

Fig. 3.19.: Logarithmic dependency of the mass for gas and DM (left) and for stars and DM (right).

subhalos. On the right side of Fig. 3.19, where the mass of the dark matter is plotted against the mass of the stars we can also see a correlation but there is a high scattering of the values around the linear line.

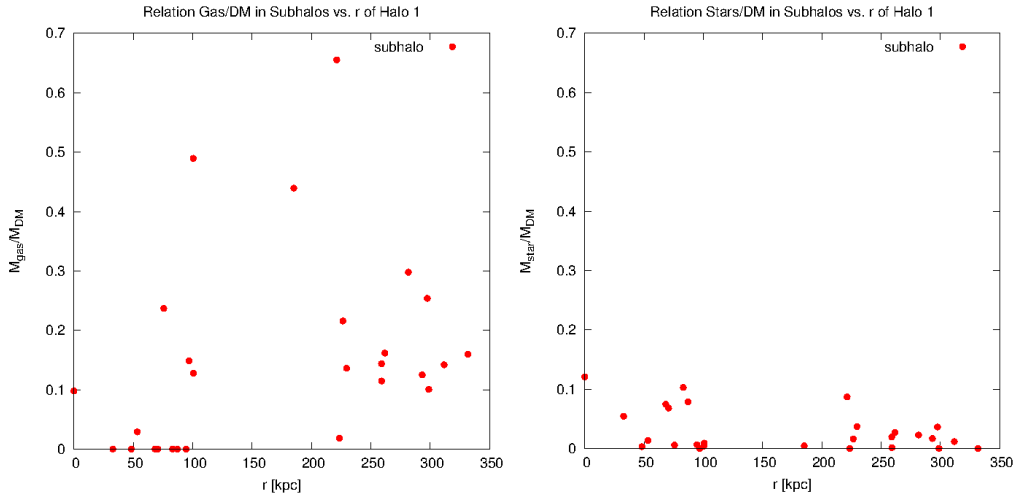

Fig. 3.20.: Relation of the mass for gas and DM (left) and for stars and DM (right) vs. $3R_{vir}$. The scales are the same to make the discrepancy clear.

Now we want to look at the relation of dark matter and gas and stars respectively regarding the position of the subhalos. Therefore we have plotted the radius against the fraction of gas mass to the dark matter mass M_{gas}/M_{DM}. On the left side of Fig. 3.20 we can see that most of the subhalos have a gas mass fraction between 10 and 20 percent. There are also two substructures that have a gas mass fraction of about 50 percent and even one substructure that has a mass ratio of M_{gas}/M_{DM} of 70 percent. Near the halo center there are some subhalos that do not have any gas. These subhalos have used all their gas to form stars and the remaining gas got stripped when the subhalo entered the virial radius. We can check this by looking at the right plot of Fig. 3.20, where we see the ratio of the star mass and the dark matter mass M_{stars}/M_{DM}. There is only one subhalo within 100 kpc that has no mass in stars. We have chosen the same scale for both relations to make it clear to see that there is in general more gas mass than stellar mass. (Note: A subhalo in one plot corresponds to the same position on the radius scale of the other plot.)

3.3. Properties at Different Redshifts

For the following section we have traced the four halos back to redshift z = 4.22 (where possible) and up to z = 0.96. Therefor we have used a tracer program and partly searched them manuelly. For a better identification we used the cold gas and if that was not enough also the distribution of the dark matter. At higher redshifts it becomes more difficult to clearly identify the central halos because they are very small and have much cold gas. Additionally there seem to be some mergers at higher redshifts that change the structures of the halos. Halo 3 and 4 could not be identified without doubt for the Snapshot 20 (z = 4.22), so we have no values for these two halos at redshift 4.22.

3.3.1. Evolution of Halo 1

In Section 3.2 we have investigated the properties of the four halos at redshift 2.33 and found that Halo 1 is a good candidate for further investigations because of its cold streams. Now we study the evolution of the streams with time.

In Fig. 3.21 and Fig. 3.22 we plotted the cold gas particles within $3R_{vir}$ of Halo 1 from redshift z = 4.22 - 0.96 beginning from the upper left to the lower right. The first thing we see is the change in the size of the halo. This growth is due to the expansion of the universe. In generel the cold gas particles become less with time because the gas is heated by the virial shock mainly caused by the AGN feedback. At some point the heating dominates the cooling of the cold streams and so the flows heat up. This consequence is shown by streams getting thinner with time, especially the flow in the upper right, finally even breaking down. Interestingly, the cold stream that breaks down first, is the smooth stream, while the clumpy stream with lots of substructures survives.

One very interesting thing, which we cannot see here in these plots is the 'wandering' of the clumps inwards along the stream. Therefore we have added Fig. C.1 in the Appendix, where the cold gas distribution for redshift 2.33 and 1.98 is shown along with the positions of the substructures. In this plot we see that for example the clump in the upper left and the cumulation of substructures in the right middle stream towards the halo center.

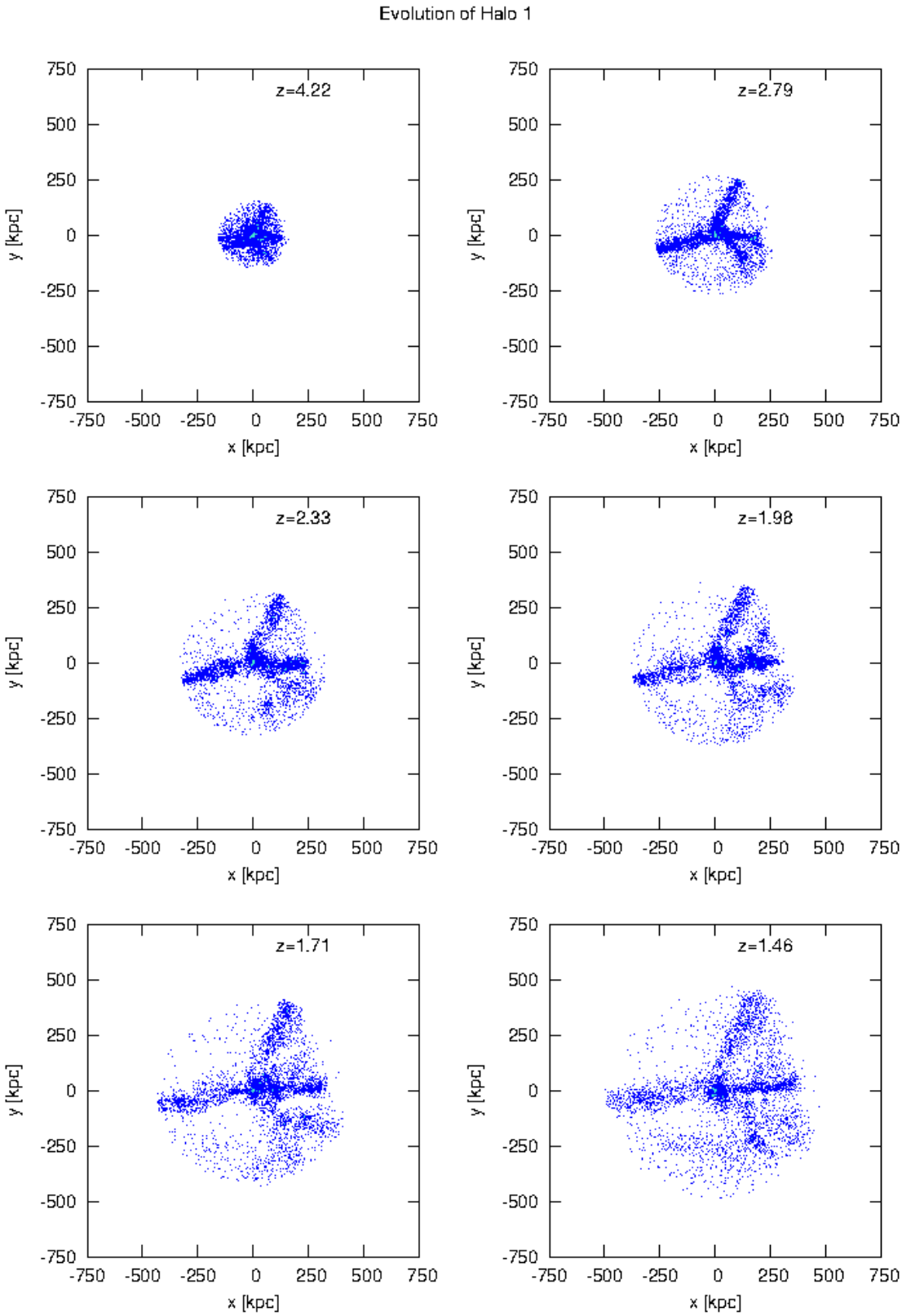

Fig. 3.21.: Evolution of Halo 1: The cold gas particles are blue and the starforming particles are turquoise, here from redshift 4.22 to 1.46

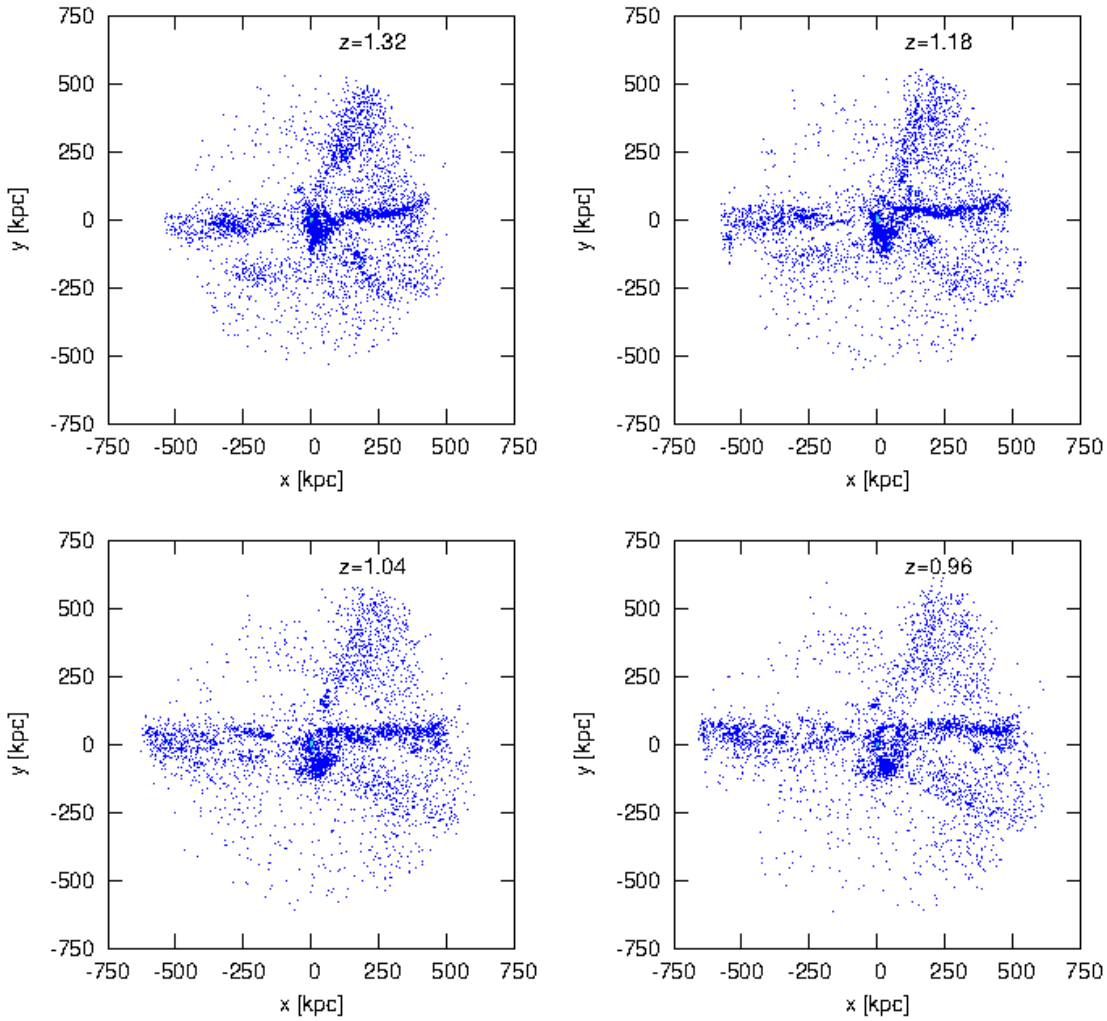

Fig. 3.22.: Evolution of Halo 1: The cold gas particles are blue and the starforming particles are turquoise, here from redshift 1.32 to 0.96

3.3.2. Massflux

We also study the change of the mass flow rate with time. Therefor the redshifts 4.22, 2.33 1.32 and 0.96 were selected and plotted for cold and hot gas.

At redshift z = 4.22 the massflux of the cold gas is relatively constant around 100 $M_\odot$/yr but peaks near the halo center. The strong starformation peak of more than 700 $M_\odot$/yr could indicate a recent, massive merger event.

This could be the reason why this halo could not be identified clearly at redshift 5.24. The net massflux for the hot gas is constant between 0 and 10 $M_\odot$/yr.

At z = 2.33 the massflux of the cold gas is between 25 and 150 $M_\odot$/yr outside R_{vir}, within R_{vir} between 25 and 70 $M_\odot$/yr, and we can see a substructure moving

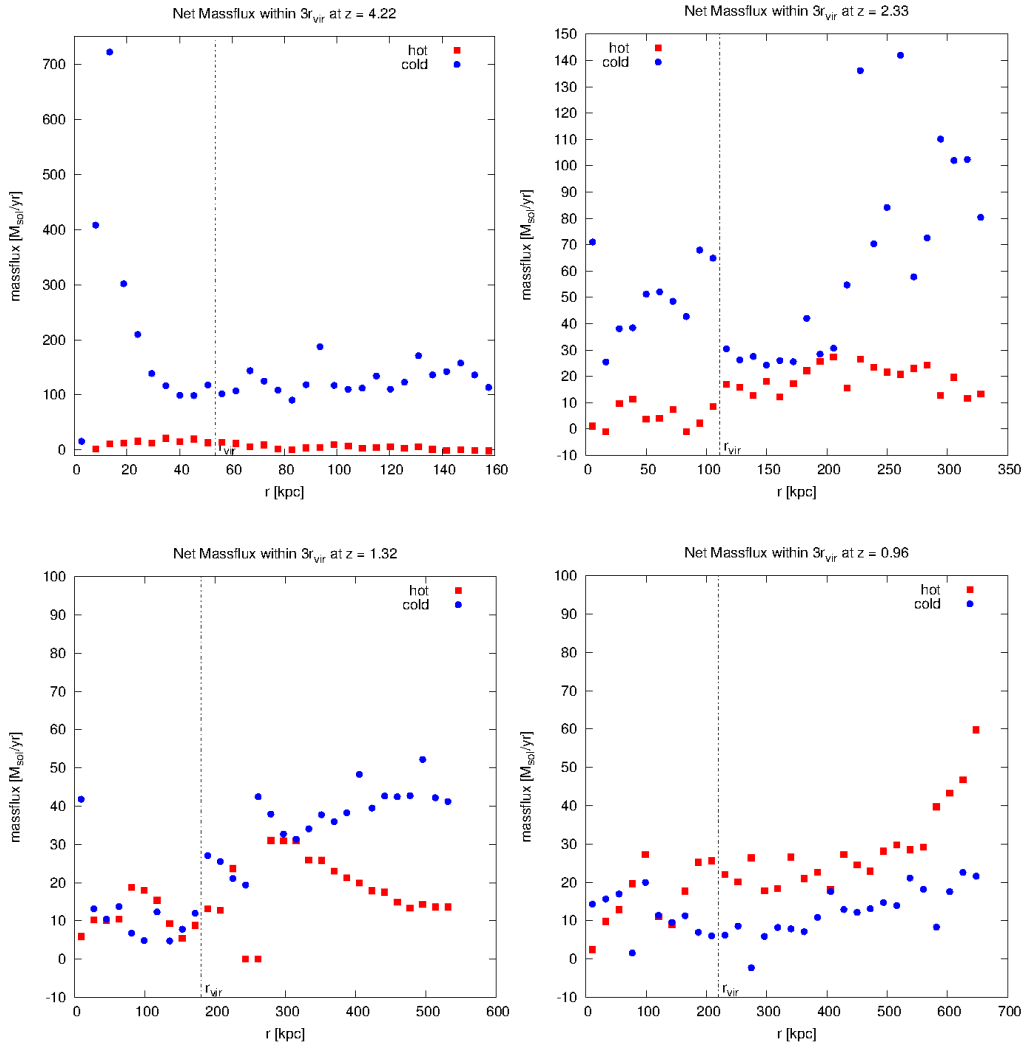

Fig. 3.23.: Massflux of cold (blue) and hot (red) gas within $3R_{vir}$ for z = 4.22, 2.33 and 0.96

inwards at r $\approx$ 250 kpc.

In the plot for redshift z = 1.32 the cold gas massflux decreases along the radius inwards and has a small peak at the center. The hot gas is seen in a curve with values between 0 and 30 $M_{\odot}$/yr. Within the virial radius the mass flow rate is between 5 and 20 $M_{\odot}$/yr.

At redshift 0.96 we see that the inflow rate of the hot gas is higher than that of the cold gas, which has values between 0 and 20 $M_{\odot}$/yr. The hot gas enters $3R_{vir}$ with 60 $M_{\odot}$/yr, then decreases, stays constant at 30 $M_{\odot}$/yr and drops to zero near the center.

In general we can say that the hot gas inflow is constant from outside till R_{vir} and decreases from the virial radius to the halo center. With time the massflux of the hot gas increases, while the massflux of the cold gas decreases.

3.3.3. Mean Temperature along Stream

In Fig. 3.22 we have seen that the streams break down and thus we want to investigate how the cold gas changes its temperature along the stream with time.

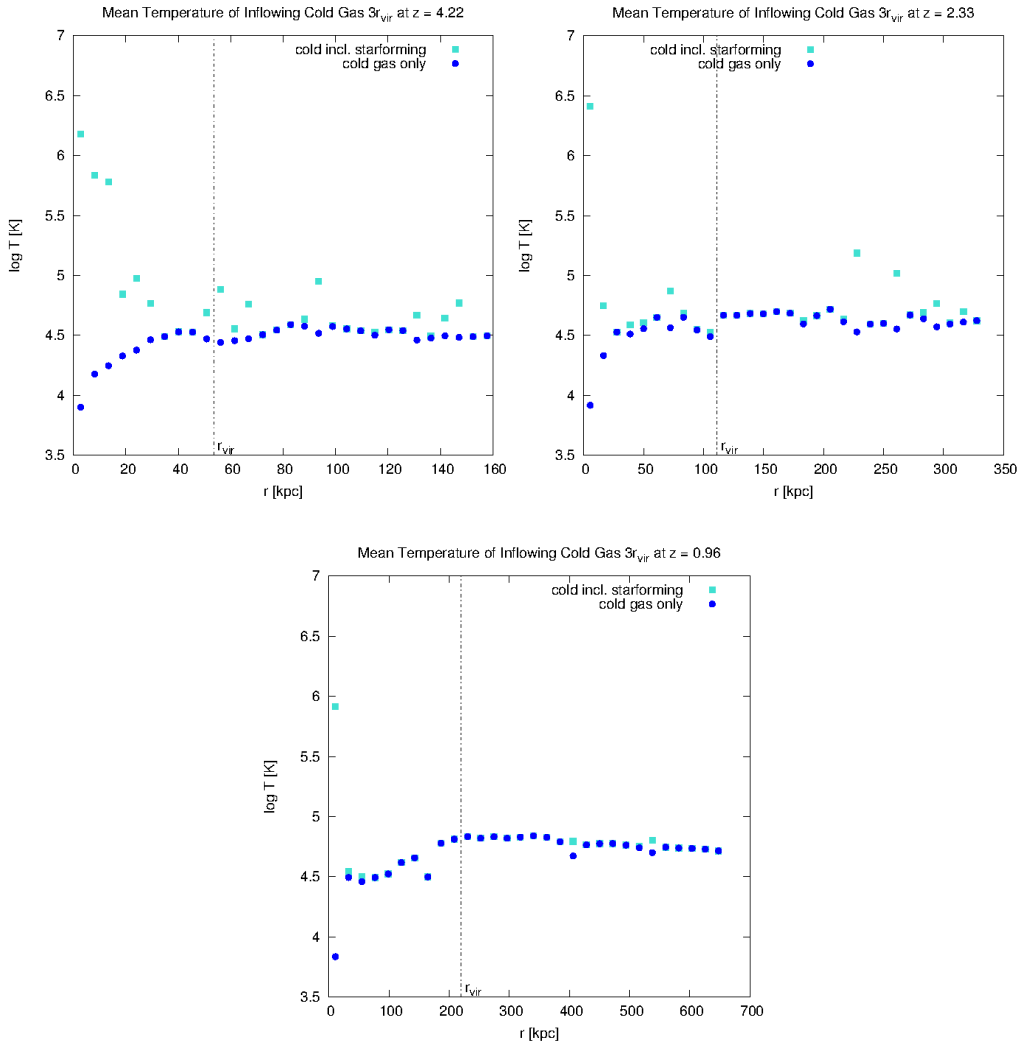

Fig. 3.24.: Massflux of cold (blue) and hot (red) gas within $3R_{vir}$ for z = 4.22, 2.33 and 0.96

Fig. 3.24 shows the radius against the mean temperature of the inflowing cold gas

particles for the redshifts 4.22, 2.33 and 0.96 for Halo 1. At z = 4.22 the cold gas particles have a constant mean temperature of $10^{4.5}$ K, dropping within the virial radius towards the center. From the plot at z = 0.96 we can conclude that the temperature along the stream heats up with time, since here the mean temperature is $10^{4.8}$ K. This matches the evolution of the cold and hot massfluxes as seen in the subsection before.

In addition Fig. 3.25 shows the number of cold particles in a temperature range between 10^4 and 10^5 K to make clear that there are less cold particles with time.

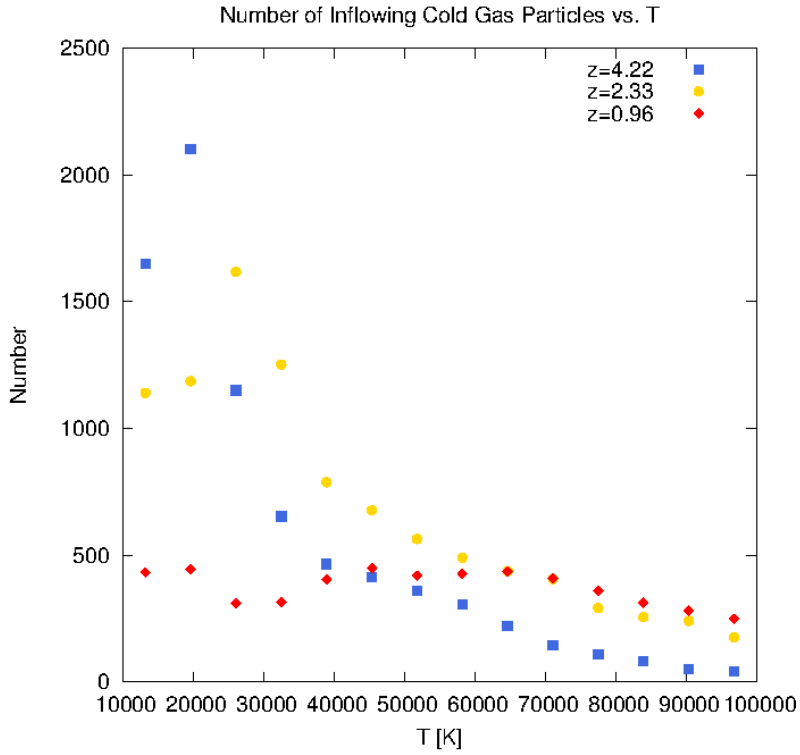

Fig. 3.25.: The number of cold inflowing particles within a temperature range [10^4 and 10^5] K for different redshifts: 4.22 (blue), 2.33 (yellow) and 0.96 (red).

At the highest redshift we see that there are many cold particles with a maximum at $2 \cdot 10^4$ K and approximately 2200 particles. For redshift 2.33 the maximum value is a little smaller with 1600 particles at $3 \cdot 10^4$ K. At redshift 0.96 there is no peak and the curve is between 250 and 500 particles. This means that with decreasing redshift the number of cold particles within a cold stream becomes fewer because the cold gas is heated up. In a plot over all temperatures we would expect a growing

peak in the number of hot particles with time. This result matches the assumption that the cold gas has been heated by the starforming particles to the intermediate warm accretion mode with temperatures between $2.5 \cdot 10^5$ and 10^6 K (Murante et al., 2012). Once the gas reaches the virial temperature it never cools due to the AGN feedback (Cattaneo et al., 2006).

3.3.4. Starformation Rate and Massflux

In the following subsection we study the relation between the starformation rate of the gas and the mean mass flow rate of the cold gas including the multiphase particles and compare it with the massflux used in Dekel et al. (2009a).

As we have already mentioned in the theoretical foundations, the starformation rate should depend on the inflowing gas. We want to probe this by examining the plots for the four halos in Fig. 3.26. Here the starformation rate is yellow, the massflux that has been derived in the theoretical basics and is used in our calculations (we will simply call it massflux or mass flow rate), given by

$$\frac{dM}{dt} = \frac{v_i m_i}{\delta r_i},$$

is blue and the massflux following Dekel et al. (2009a), given by

$$\dot{M} \simeq 6.6 M_{12}^{1.15} (1+z)^{2.25} f_{.165} M_{\odot} yr^{-1},$$

is red.

In general we see that the mass flow rate according to Dekel et al. (2009a) is higher than the mass flow rate. The other thing is that the starformation rate follows the massflux.

The massflux of Halo 1 is high at redshift 4.22 with 160 $M_{\odot}$/yr and then drops linearly with time. The massflux following Dekel et al. (2009a) has almost the same behavior. At z = 4.22 there are ≈180 $M_{\odot}$/yr inflowing and the massflux increases up to ≈195 $M_{\odot}$/yr and is then decreasing linearly. We can see that the starformation rate is around 40 $M_{\odot}$/yr, then increases up to 80 $M_{\odot}$/yr. This increase of the starformation rate could be the result of the major merger in the center the halo is undergoing between redshift 4.22 and 2.79. Then the starformation rate follows the dropping massflux.

Halo 2 shows a slightly different picture. The massflux is low at z = 4.22 with ∼50

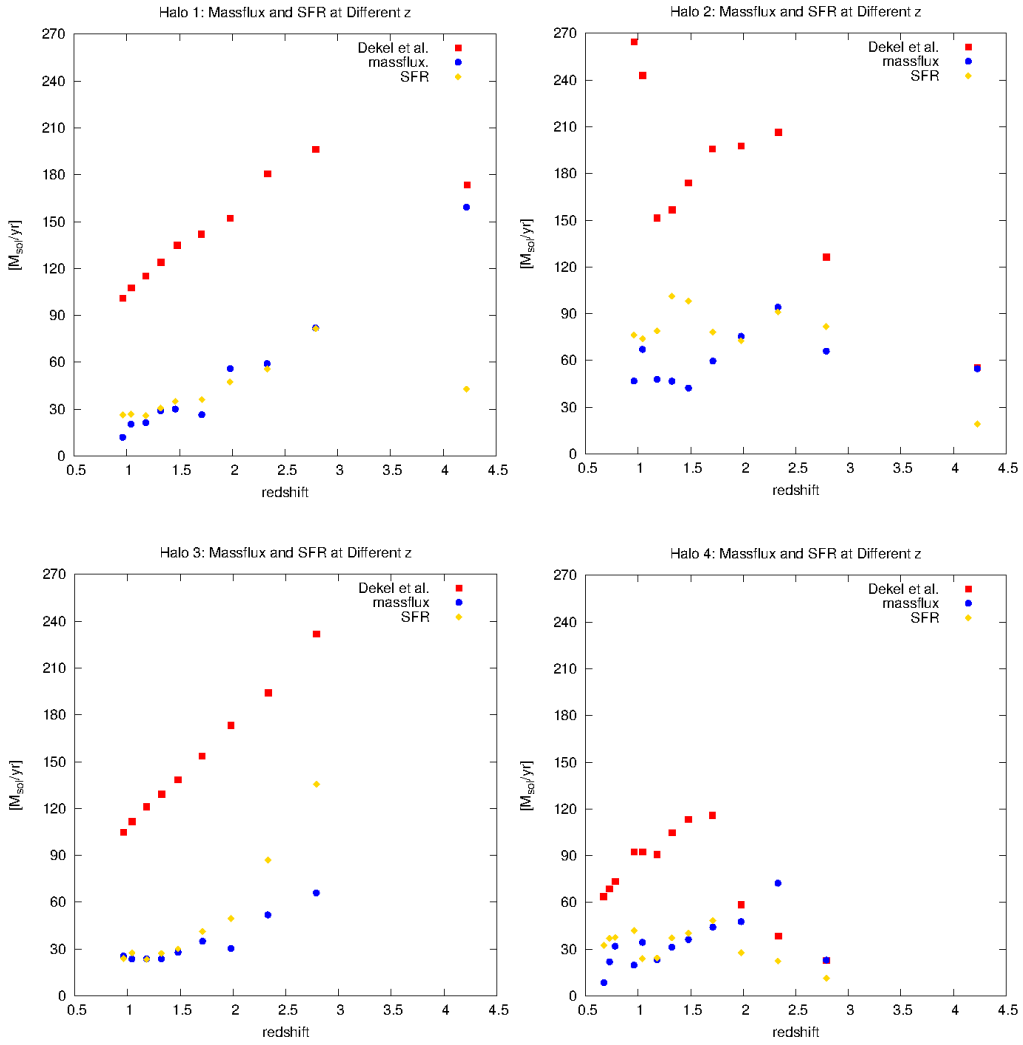

Fig. 3.26.: Massflux calculated with formula from Dekel et al. (2009a)(red), massflux as calculated before (blue) and starformation rate of the gas (yellow)

$M_\odot$/yr. It increases up to ∼100 $M_\odot$/yr at z = 2.33, then drops till z = 1.46 under ≈50 $M_\odot$/yr and has a small peak at redshift 1.04 with ∼70 $M_\odot$/yr. The massflux curve following Dekel et al. (2009a) has a similar shape but is higher by a factor of ∼3. The values of the starformation rate are in the range of the mass flow rate but seem delayed. As seen for Halo 1, Halo 2 also has a merger between redshift 1.98 and 1.71 that seems to trigger the starformation, which increases at z = 1.46.

The shape of the curve in the plot for Halo 3 shows a similar picture to that of Halo 1. The massflux at z = 2.79 is around 65 $M_\odot$/yr and is linearly dropping. So

does the massflux following Dekel et al. (2009a) besides it is higher by a factor of 3-4. Interestingly the starformation rate is higher than the mass flow rate. This could be due to the time delay of the starformation according to the cold gas inflow rate. Since the massflux is so low compared to the starformation rate, we assume that there could have been a merger in the past that had triggered this high starformation rate with $\sim$140 $M_\odot$/yr at redshift 2.79.

The mass flow rate of Halo 4 is increasing between redshift 2.79 and 2.33 from 30 to 80 $M_\odot$/yr, which could be due to the incoming merger, and then dropping under 30 $M_\odot$/yr at z = 1.18. The massflux following Dekel et al. (2009a) also starts with 30 $M_\odot$/yr at z = 2.79 and then increases up to 120 $M_\odot$/yr at redshift 1.71 and decreases from that point. The starformation rate has its maximum at z = 1.71 with $\sim$45 $M_\odot$/yr. There are mergers, the first between 1.98 and 1.71 and the second between 1.32 and 1.17. As seen before this leads to an increasing starformation rate at z = 1.71 and a little delayed at z = 0.96.

To see the relation between the starformation rate and the massflux of cold gas directly we have plotted them in Fig. 3.27, where every red point stands for a redshift and the straight line is the fit function.

For the plot of Halo 1 we have skipped the values for redshift 4.22 because this point was extremely outlying. We can see a good correlation between the massflux and the staformation rate and that the massflux is slightly higher than the starformation rate.

Halo 2 does not show such a correlation. Here the values cumulate at a section of the straight line. The value at (massflux in $M_\odot$/yr: 54, SFR in $M_\odot$/yr: 19) is the one at redshift z = 4.22.

In the plot for Halo 3 we see a strong correlation again but this time the starformation rate is higher than the massflux, as seen before.

The values for Halo 4 do not have such a strong correlation. They gather around a section of the fitted straight line, similar to Halo 2.

We conclude that in general the starformation rate is correlated to the mass flow rate for redshifts smaller than 4. It seems like the starformation is not correlated to the massflux at z$\gtrapprox$4 or there might be a correlation by another factor than at lower redshifts.

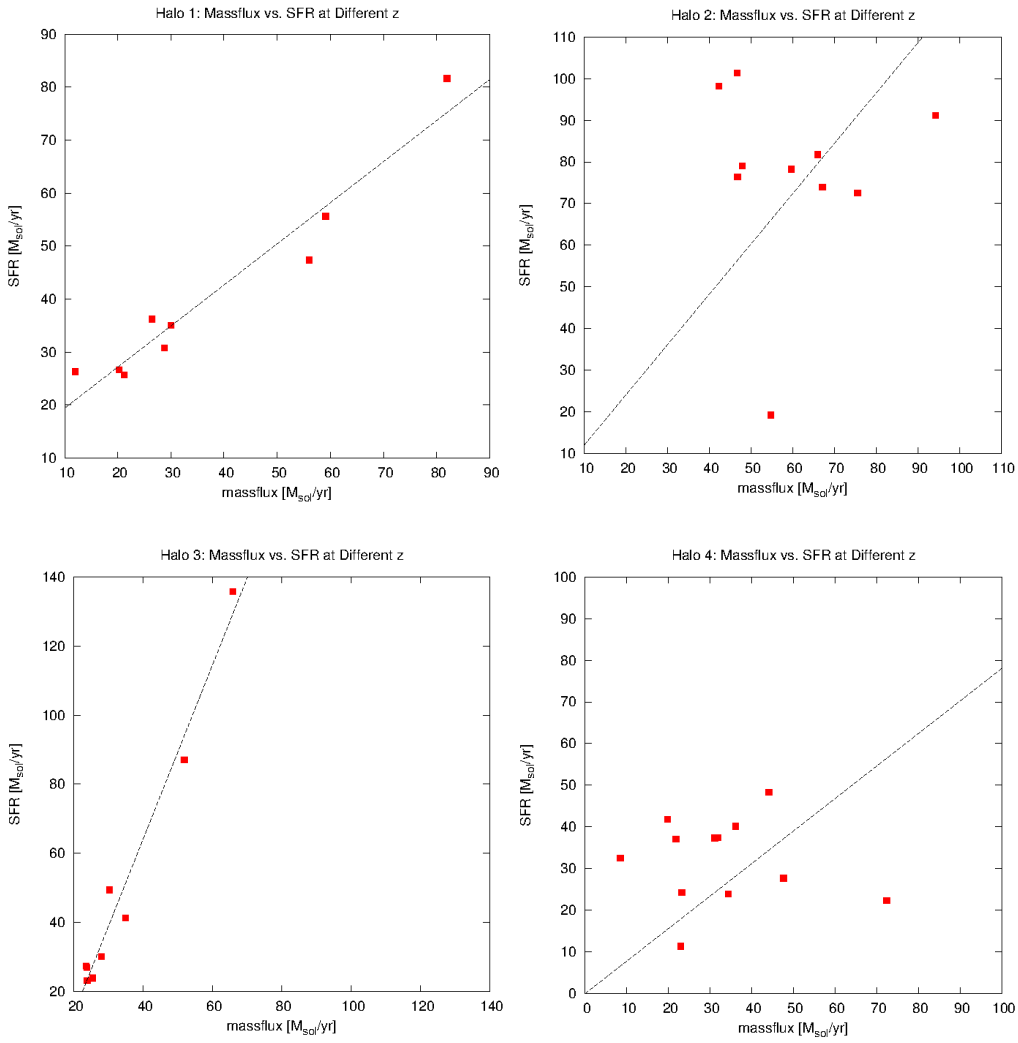

Fig. 3.27.: Here massflux is plotted against the starformation rate.

3.3.5. Subhalos of Halo 1

In subsection 3.2.8 we have seen that two of the three streams seen in the xy-plane have only one subhalo at z = 2.33, unlike the stream in the right middle, which has many substructures. To investigate if this changes in time and if these two streams are smooth cold flows at all redshifts we have plotted the distribution of cold gas in blue and the subhalos in yellow for the redshifts 2.79, 1.32 and 0.96.

In this sequence we see that the stream in the upper right has only very few substructures over all observed times, i.e. this cold flow is smooth. The left and the right stream in the middle have subhalos at all times.

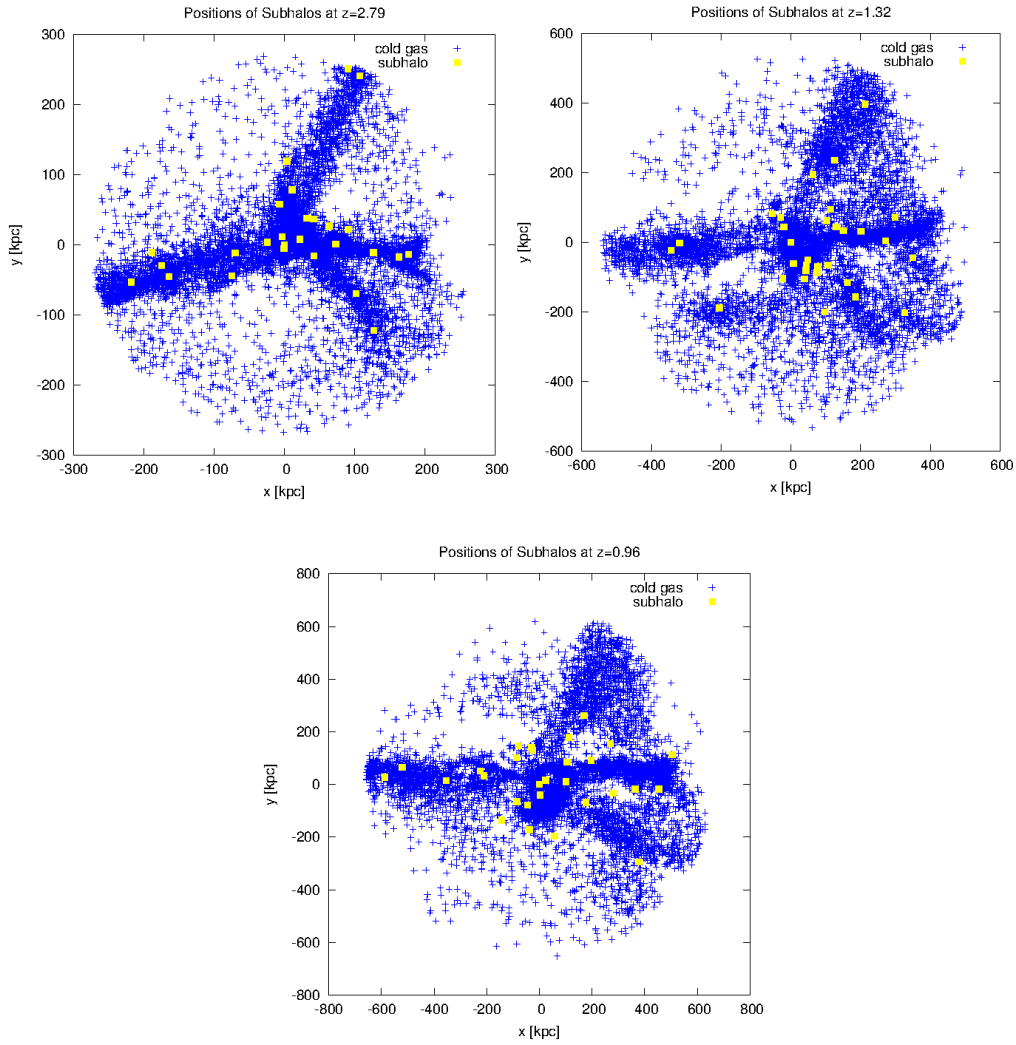

Fig. 3.28.: Halo 1 at redshifts 2.79, 1.32 and 0.96. The cold gas is blue and the subhalos are yellow.

At last we want to see if there is a pattern in the distribution of the subhalos within $3R_{vir}$ concerning their mass ratio M_{gas}/M_{DM} and M_{stars}/M_{DM}. Therefor we have plotted the radius against the mass ratio for the redshifts 2.79, 1.32 and 0.96.

In Fig. 3.29 we see no relation between the M_{gas}/M_{DM} mass ratio and the distance to the center of the halo at redshift 2.79. There are three subhalos that have between 40 and 50 percent gas mass. At z = 1.32 there is apparently less gas and a lot of subhalos do not have any gas. Here the maximum value has decreased to 30 percent. This tendency is also seen in the plot for redshift 0.96, where the maximum is 15 percent and there are many substructures without gas, too. We note that this does

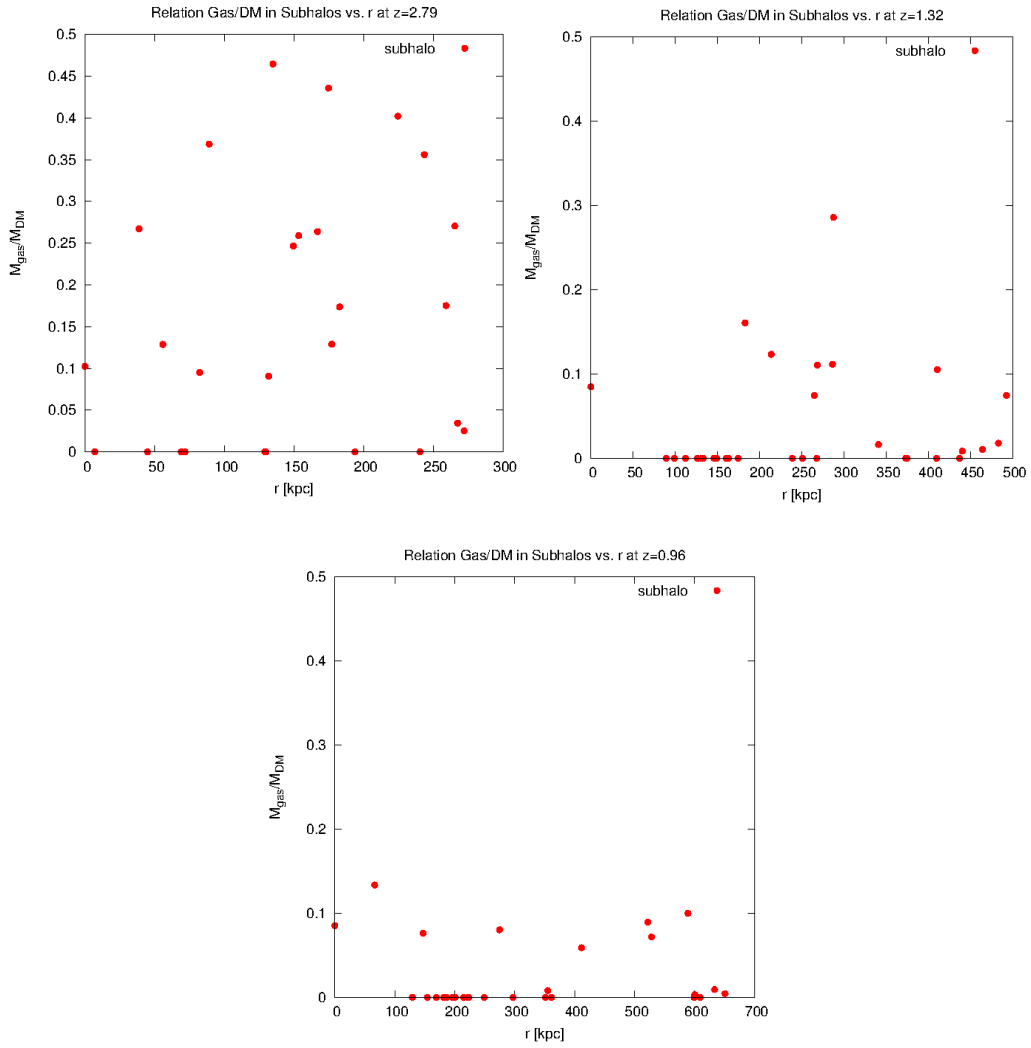

Fig. 3.29.: The mass ratio M_{gas}/M_{DM} for Halo 1 at redshifts 2.79, 1.32 and 0.96. Every point represents a subhalo at radius r.

not depend on the distance to the halo center and that the main galaxy holds the same value of about 10 percent through all times.

Fig. 3.30 shows the stars - dark matter mass ratio. At redshift 2.79 one subhalo has a mass ratio M_{stars}/M_{DM} around 40 percent, and the other values lie under 13 percent. Some of the substructures show more stars at z = 1.32 than in the higher redshift. The reason for this is that the gas from these subhalos has turned into stars and now these substructures only consist of 'stripped stars'. But on the other hand we also see subhalos that have no stars. For lower redshift as here z = 0.96 the maximum in the mass of stars decreases. In general we note that here, too,

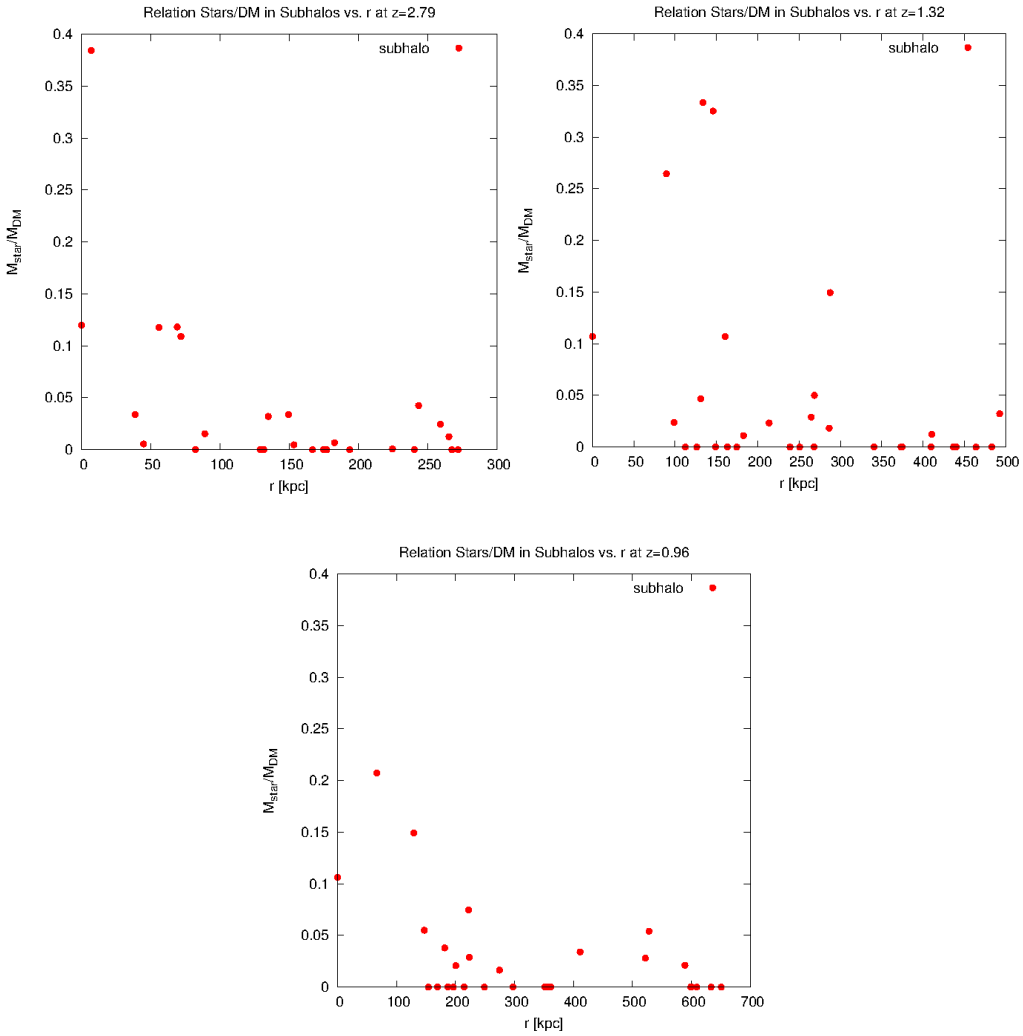

Fig. 3.30.: The mass ratio M_{stars}/M_{DM} for Halo 1 at redshifts 2.79, 1.32 and 0.96. Every point represents a subhalo at radius r.

the subhalos that do not have any stars, are distributed without a pattern over the whole $3R_{vir}$ and that the main galaxy keeps a constant value.

Summary

We briefly want to summarize the results of the investigations of the four halos at the redshifts 4.23 to 0.96.

First we have looked at the halos at z = 2.33 and have seen the flows of cold gas heading to the halo center. The cold streams come in from the filaments of the cosmic web and follow the dark matter distribution. In these cold flows, starforming regions move embedded in clumps of cold gas inwards. It seems like the formation of the stars is not finished until they reach the halo center, since the starformation takes place mainly in the center. The hot gas is spread spherically symmetric around the halo center and partly surrounds the cold streams.

The pressure of the cold and the hot gas is in equilibrium between $3R_{vir}$ and R_{vir}. Within R_{vir}, the hot gas has a higher pressure due to the gravitational force it has to compensate to gain equilibrium.

The density of the 'smooth' cold gas is only slightly higher than that of the hot gas. The substructures peak out in the density vs. radius diagram due to the fact that they are very dense, starforming regions.

The net massflux of the hot gas along the radius is very low at high redshifts and increases with time. The outflow of hot gas near the halo center indicates a strong AGN feedback, as seen in halo 2. At high redshifts the mass flow rate of the cold gas along the radius is high, especially where substructures are seen. For the cold gas we almost see no outflow, so the inflow rate dominates the net massflux. With time the cold massflux decreases and at redshift 0.96 it is even less than the hot massflux. If we compare the mass flow rates over the different reshifts we find the maxima for halo 1 at z = 4.23, halo 2 and 4 at z = 2.33 and for halo 3 at z = 2.79.

We have seen that the starformation rate seems to follow the mass flow rate with a time delay. The curve for the massflux as proposed by Dekel et al. (2009a) has a similar shape but is higher by a factor of about 3-4 than the here used formula of the mass flow rate.

The mean temperature along a cold stream is almost constant between $3R_{vir}$ and R_{vir} and then decreases until it reaches the center of the halo. We also see a slight drop at the positions where stars are about to form. Over the time the cold stream becomes warmer, since the number of cold particles decreases.

We have also investigated the subhalos and find that there is a logarithmic dependency of the mass ratio M_{gas}/M_{DM} and M_{stars}/M_{DM}. By comparing the subhalos position along the radius with the mass ratio M_{gas}/M_{DM} we see that there is less gas with time, since it converts to stars. From the same diagram with the mass ratio M_{stars}/M_{DM} we learn that at high redshifts there are few stars, then the mass of stars in the subhalos increase slighly and then there are less stars with time. For both ratios we learn that it does apparently not depend on the distance to the center, whether there is gas (and respectively stars) or not and that the main halo keeps the same value at all investigated reshifts.

The constraints at high redshift, under which disks form, have to be investigated in further studies. We conclude from the evolution of the massflux over time that it is likely that disks are built by clumpy infall. Halo 1, which has beautiful smooth streams with only small clumps at high redshifts, does not form a disk at lower redshifts. On the other hand, Halo 4 has a beautiful, extended disk at z = 0.96 (see Bachelor Thesis of Felix Schulze). Thus we conclude at first sight that the halos with a 'turbulent', clumpy mass flow rate over time and mergers between redshift 2 and 1 (here Halo 2 and 4) have disks at lower redshifts, while smooth accretion cannot produce disklike structures within our resolution limits. To see if this can be generalized, the evolution and properties of many halos need to be analyzed.

Another aim is to find these cold streams at high redshifts in observations. One reason for the difficulty in detecting the cold flows at high redshifts might be the intermediate warm accretion mode with temperatures between $2.5 \cdot 10^5$ and 10^6 K, as discussed by Murante et al. (2012). Fumagalli et al. (2011) conclude that it should be possible to detect cold streams in the absorption lines of quasars and galaxy pairs. The inflowing gas might be distinguished from the outflowing gas by chemical composition (e.g. metallicity) and kinematics (e.g. velocity) (see also Faucher-Giguère and Kereš (2011)) but it is expected that the signatures of the cold streams are much weaker than those of the outflowing gas (Goerdt et al., 2012).

Acknowledgements

First of all I would like to thank Prof. Dr. Andreas Burkert for this interesting and fascinating matter.

Then special thanks go to Dr. Klaus Dolag and Rhea-Silvia Remus for their patience and the time, they have taken to help me understand the matter and Katharina Fierlinger for her help with gnuplot.

I also like to thank my children, who gave me the strength to look forward throughout my whole studies, and my husband, who encouraged me to study physics and always believed in me.

Another thank-you goes to Andreas Schmidt, who helped me solve some questions concerning the programming and who supported me throughout the whole studies.

I would also like to thank the other bachelor students Felix Schulze, Torben Simm and Lucas Sommer for their tips and help.

Last but not least I want to thank my grandfather, my mother, who awakened my interest in astronomy, and my friends, especially Jessica Gettkandt and Florian Semrau, who persuaded me to study physics.

A. Appendix: Tables

In Tab. A.1 to Tab. A.4 we have listed some data for the halos between redshift 4.23 and 0.96. The stellar, gas and DM masses refer to the particles within the virial radius.

We see that the fraction of the dark matter mass is constant at all redshifts. The cold gas fraction decreases with time, on the other hand the fraction of the hot gas increases.

Tab. A.1.: Halo 1

Redshift	4.227	2.791	2.334	1.323	0.962
r_{vir}/kpc	53.4691	91.5427	111.069	180.184	219.543
$m_{vir}/M_{\odot}$	$6.14219 \cdot 10^{11}$	$1.19459 \cdot 10^{12}$	$1.46817 \cdot 10^{12}$	$2.26065 \cdot 10^{12}$	$2.60778 \cdot 10^{12}$
m_{star}/m_{vir}	0.0286392	0.0759445	0.0759068	0.0725844	0.0715641
m_{gas}/m_{vir}	0.126668	0.0902991	0.0860784	0.0813839	0.0837999
m_{DM}/m_{vir}	0.84475	0.833791	0.837974	0.846032	0.844593
m_{cold}/m_{gas}	0.459449	0.377521	0.322096	0.170782	0.123865
m_{hot}/m_{gas}	0.120923	0.449017	0.530195	0.751349	0.797468
m_{sf}/m_{gas}	0.419671	0.178053	0.157225	0.0813147	0.0814806

Tab. A.2.: Halo 2

Redshift	4.227	2.791	2.334	1.323	0.962
r_{vir}/kpc	39.124	83.4861	118.262	190.814	293.966
$m_{vir}/M_{\odot}$	$2.40622 \cdot 10^{11}$	$9.06172 \cdot 10^{11}$	$1.77213 \cdot 10^{12}$	$2.68496 \cdot 10^{12}$	$6.2606 \cdot 10^{12}$
m_{star}/m_{vir}	0.0232409	0.040717	0.0454566	0.0673874	0.0623326
m_{gas}/m_{vir}	0.123878	0.10915	0.105545	0.0914032	0.0871803
m_{DM}/m_{vir}	0.852874	0.850129	0.848959	0.841208	0.850463
m_{cold}/m_{gas}	0.557835	0.468324	0.399211	0.209556	0.126719
m_{hot}/m_{gas}	0.0694544	0.293216	0.452667	0.686931	0.795454
m_{sf}/m_{gas}	0.372711	0.2398	0.154397	0.10575	0.080934

Tab. A.3.: Halo 3

Redshift	2.791	2.334	1.323	0.962
r_{vir}/kpc	97.1061	110.485	179.237	220.948
$m_{vir}/M_{\odot}$	$1.42582 \cdot 10^{12}$	$1.44507 \cdot 10^{12}$	$2.22524 \cdot 10^{12}$	$2.65804 \cdot 10^{12}$
m_{star}/m_{vir}	0.0651335	0.0886729	0.0823929	0.0756851
m_{gas}/m_{vir}	0.0960593	0.0859027	0.0795371	0.0816313
m_{DM}/m_{vir}	0.838808	0.825418	0.838092	0.842654
m_{cold}/m_{gas}	0.351304	0.266163	0.132197	0.0914926
m_{hot}/m_{gas}	0.455993	0.604042	0.799112	0.853929
m_{sf}/m_{gas}	0.199272	0.13555	0.0741376	0.0585939

Tab. A.4.: Halo 4

Redshift	2.791	2.334	1.323	0.962
r_{vir}/kpc	50.1094	72.4263	171.526	209.629
$m_{vir}/M_{\odot}$	$1.9593 \cdot 10^{11}$	$4.07031 \cdot 10^{11}$	$1.95041 \cdot 10^{12}$	$2.27034 \cdot 10^{12}$
m_{star}/m_{vir}	0.0298409	0.0255568	0.0408059	0.046718
m_{gas}/m_{vir}	0.125733	0.126242	0.113292	0.118167
m_{DM}/m_{vir}	0.844418	0.848097	0.845883	0.835095
m_{cold}/m_{gas}	0.72916	0.573709	0.358565	0.309705
m_{hot}/m_{gas}	0.117	0.217028	0.542516	0.594626
m_{sf}/m_{gas}	0.169525	0.214531	0.109016	0.101458

B. Appendix: Distribution of the Components

In the plots of Fig. B.1 to Fig. B.3 we see the distribution of the components seperately plotted for the Halos 2, 3 and 4. Dark matter is black, the hot gas is red, the cold gas is navy, the multiphase particles are turquoise and the stars are yellow.

In Fig. B.4 we see the components plotted together for Halos 2, 3 and 4. Halo 2 is projected onto the yz-plane and Halos 3 and 4 are projected onto the xy-plane.

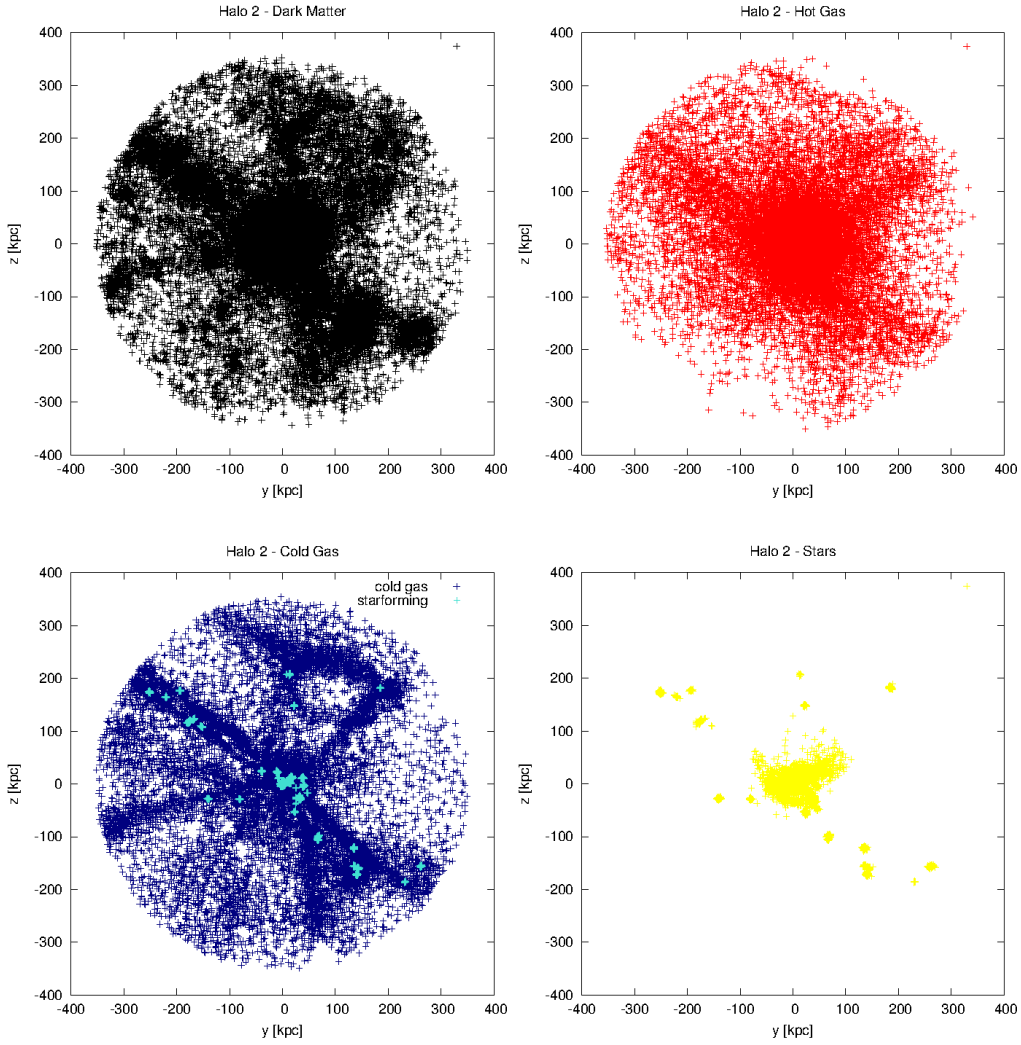

Fig. B.1.: Components of Halo 2 in the $3R_{vir}$ projected onto the yz-plane: upper left: dark matter, upper right: hot gas, lower left: cold gas incl. starforming multiphaseparticles, lower right: stars

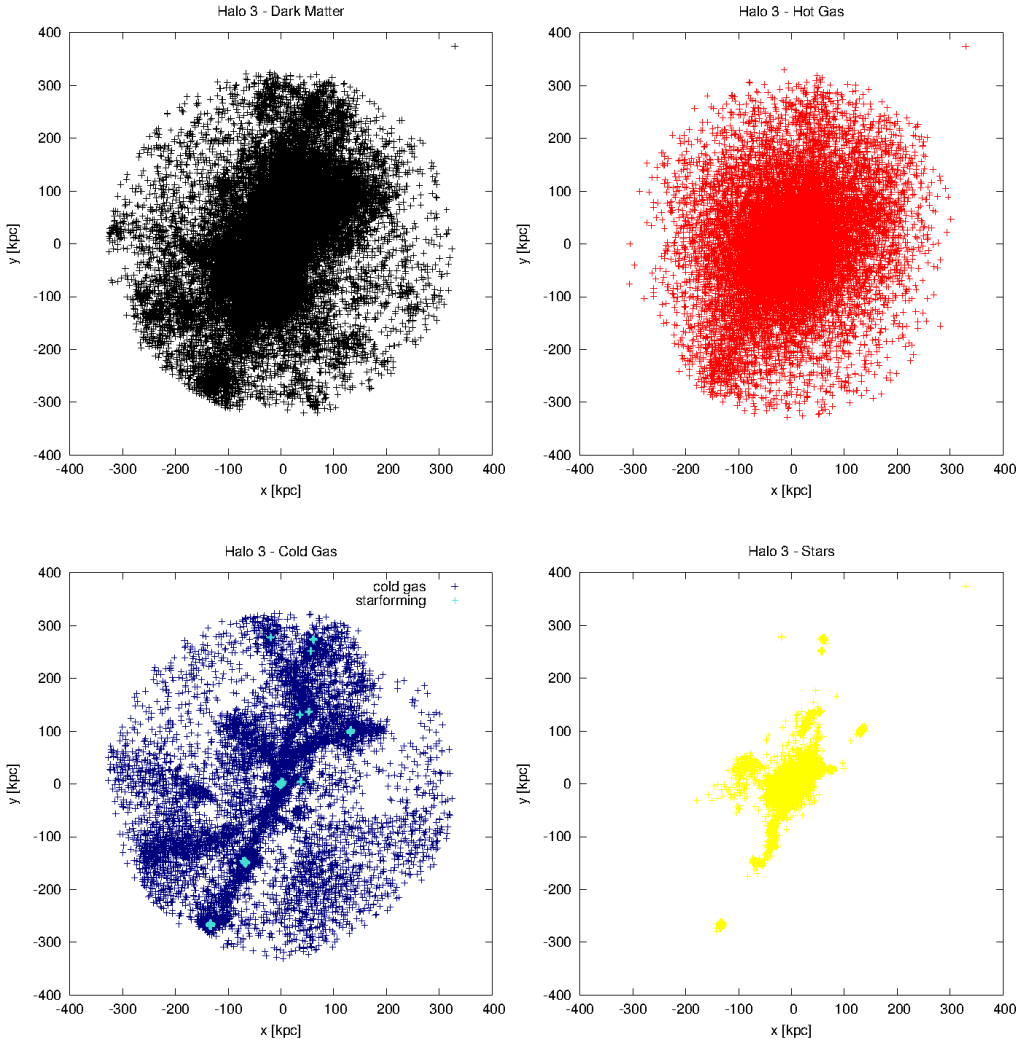

Fig. B.2.: Components of Halo 3 within three times the virial radius projected onto the xy-plane: upper left: dark matter, upper right: hot gas, lower left: cold gas incl. starforming multiphaseparticles, lower right: stars

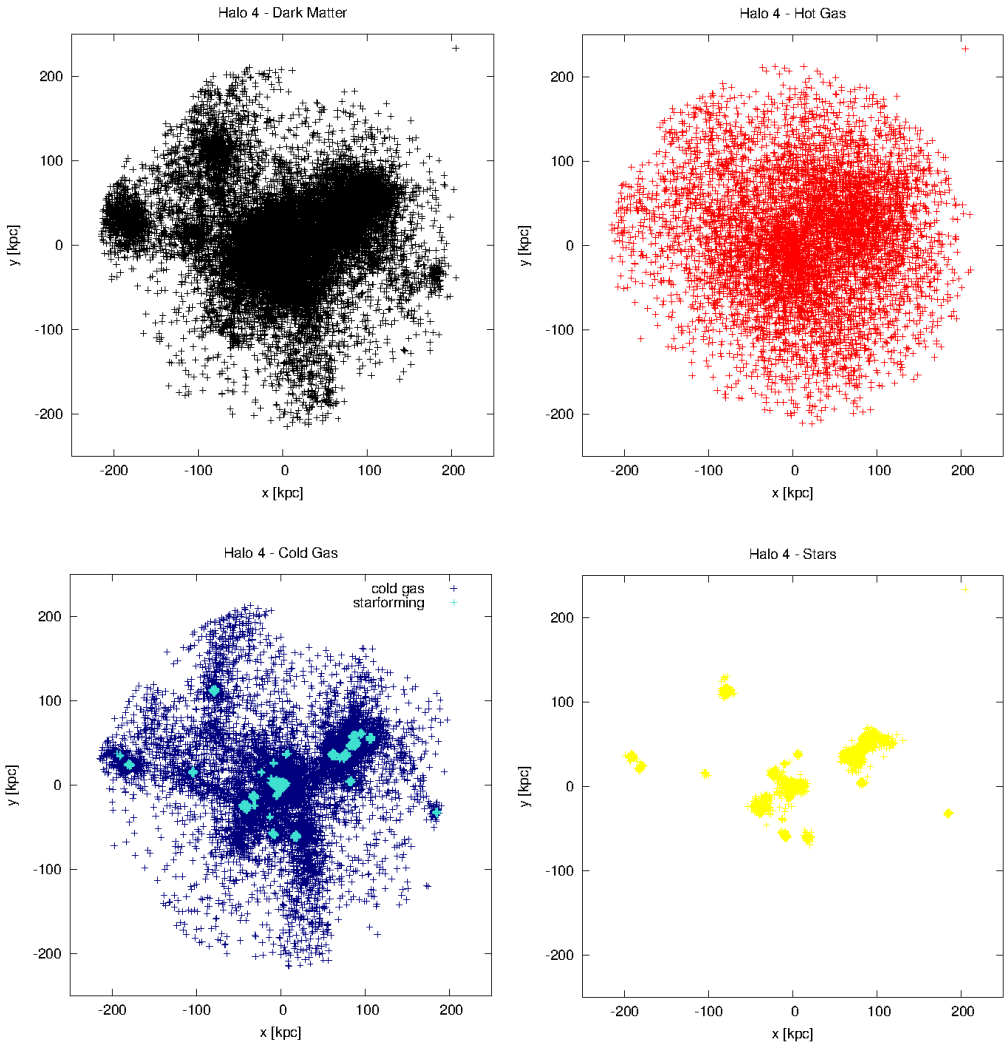

Fig. B.3.: Components of Halo 4 within $3R_{vir}$ projected onto the xy-plane: upper left: dark matter, upper right: hot gas, lower left: cold gas incl. starforming multiphaseparticles, lower right: stars

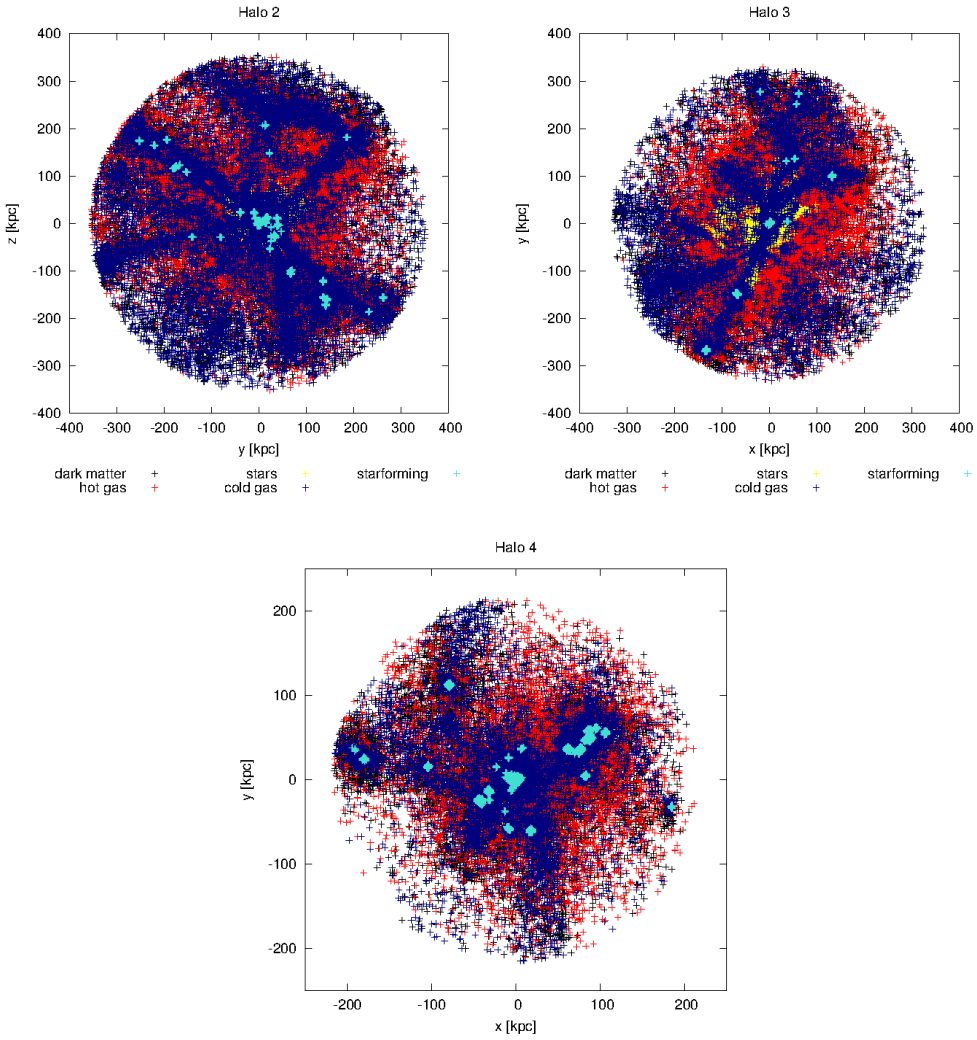

Fig. B.4.: All components of Halos 2, 3 and 4 within the $3R_{vir}$ plotted together. The components of Halo 2 are projected onto the yz-plane, whereas Halos 3 and 4 are projected onto the xy-plane. Black is dark matter, red is the hot gas, navy is the cold gas, turquoise are the starforming particles and the stars are yellow.

C. Appendix: Wandering of Clumps

Here we see the the 'wandering' of the clumps for Halo 1. We have to follow the turquoise starforming regions to see that the clumps are moving inwards.

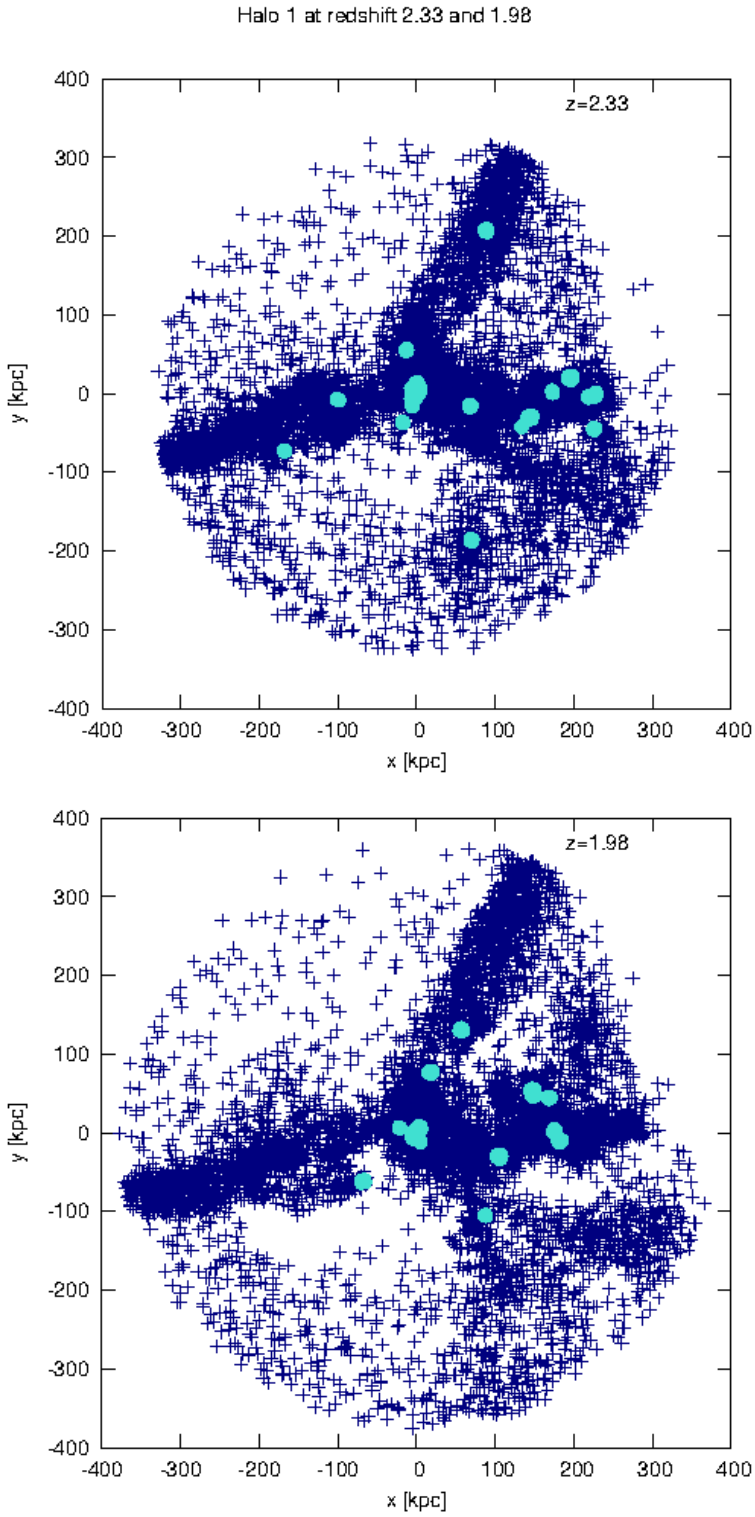

Fig. C.1.: Evolution of Halo 1: The cold gas particles are navy and the starforming particles are turquoise. The cold clumps move inwards. This cannot be seen directly in this plot but by following the straforming particles which are embedded in the clumps of cold gas. The clump in the upper right at z = 2.33 has moved a little towards the center by z = 1.98.

Bibliography

Berlind, A. A., Frieman, J., Weinberg, D. H., Blanton, M. R., Warren, M. S., Abazajian, K., Scranton, R., Hogg, D. W., Scoccimarro, R., Bahcall, N. A., Brinkmann, J., Gott, III, J. R., Kleinman, S. J., Krzesinski, J., Lee, B. C., Miller, C. J., Nitta, A., Schneider, D. P., Tucker, D. L., Zehavi, I., and SDSS Collaboration (2006). Percolation Galaxy Groups and Clusters in the SDSS Redshift Survey: Identification, Catalogs, and the Multiplicity Function. *Astrophysical Journal Supplement Series*, 167:1–25.

Binney, J. and Tremaine, S. (2008). *Galactic Dynamics*. Princeton University Press, second edition.

Bolton, J. S., Haehnelt, M. G., Warren, S. J., Hewett, P. C., Mortlock, D. J., Venemans, B. P., McMahon, R. G., and Simpson, C. (2011). How neutral is the intergalactic medium surrounding the redshift z = 7.085 quasar ULAS J1120+0641? *Monthly Notices of the Royal Astronomical Society*, 416:L70–L74.

Bouché, N., Dekel, A., Genzel, R., Genel, S., Cresci, G., Förster Schreiber, N. M., Shapiro, K. L., Davies, R. I., and Tacconi, L. (2010). The Impact of Cold Gas Accretion Above a Mass Floor on Galaxy Scaling Relations. *The Astrophysical Journal*, 718:1001–1018.

Carlberg, R. G., Yee, H. K. C., Ellingson, E., Morris, S. L., Abraham, R., Gravel, P., Pritchet, C. J., Smecker-Hane, T., Hartwick, F. D. A., Hesser, J. E., Hutchings, J. B., and Oke, J. B. (1997). The Average Mass Profile of Galaxy Clusters. *The Astrophysical Journal*, 485:L13.

Carroll, B. W. and Ostlie, D. A. (2007). *An Introduction to Modern Astrophysics*. Pearson Education Inc., second edition.

Cattaneo, A., Dekel, A., Devriendt, J., Guiderdoni, B., and Blaizot, J. (2006). Modelling the galaxy bimodality: shutdown above a critical halo mass. *Monthly Notices of the Royal Astronomical Society*, 370:1651–1665.

Dekel, A. and Birnboim, Y. (2006). Galaxy bimodality due to cold flows and shock heating. *Monthly Notices of the Royal Astronomical Society*, 368:2–20.

Dekel, A., Birnboim, Y., Engel, G., Freundlich, J., Goerdt, T., Mumcuoglu, M., Neistein, E., Pichon, C., Teyssier, R., and Zinger, E. (2009a). Cold streams in early massive hot haloes as the main mode of galaxy formation. *Nature*, 457:451–454.

Dekel, A., Sari, R., and Ceverino, D. (2009b). Formation of Massive Galaxies at High Redshift: Cold Streams, Clumpy Disks, and Compact Spheroids. *The Astrophysical Journal*, 703:785–801.

Dolag, K., Vazza, F., Brunetti, G., and Tormen, G. (2005). Turbulent gas motions in galaxy cluster simulations: the role of smoothed particle hydrodynamics viscosity. *Monthly Notices of the Royal Astronomical Society*, 364:753–772.

Fabjan, D., Borgani, S., Tornatore, L., Saro, A., Murante, G., and Dolag, K. (2010). Simulating the effect of active galactic nuclei feedback on the metal enrichment of galaxy clusters. *Monthly Notices of the Royal Astronomical Society*, 401:1670–1690.

Faucher-Giguère, C.-A. and Kereš, D. (2011). The small covering factor of cold accretion streams. *Monthly Notices of the Royal Astronomical Society*, 412:L118–L122.

Fumagalli, M., Prochaska, J. X., Kasen, D., Dekel, A., Ceverino, D., and Primack, J. R. (2011). Absorption-line systems in simulated galaxies fed by cold streams. *Monthly Notices of the Royal Astronomical Society*, 418:1796–1821.

Goerdt, T., Dekel, A., Sternberg, A., Gnat, O., and Ceverino, D. (2012). Detectability of cold streams into high-redshift galaxies by absorption lines. *Monthly Notices of the Royal Astronomical Society*, page 3314.

Hetznecker, H. (2007). *Expansionsgeschichte des Universums*. Spektrum Akademischer Verlag, first edition.

Hetznecker, H. (2008). *Kosmologische Strukturbildung*. Spektrum Akademischer Verlag, first edition.

Klessen, R. (2007). *Sternentstehung*. Spektrum Akademischer Verlag, first edition.

Komatsu, E., Smith, K. M., Dunkley, J., Bennett, C. L., Gold, B., Hinshaw, G., Jarosik, N., Larson, D., Nolta, M. R., Page, L., Spergel, D. N., Halpern, M., Hill, R. S., Kogut, A., Limon, M., Meyer, S. S., Odegard, N., Tucker, G. S., Weiland, J. L., Wollack, E., and Wright, E. L. (2011). Seven-year Wilkinson Microwave Anisotropy Probe (WMAP) Observations: Cosmological Interpretation. *Astrophysical Journal Supplement Series*, 192:18.

Landau, L. D. and Lifschitz, E. M. (1991). *Lehrbuch der theoretischen Physik, Bd. VI, Hydrodynamik*. Akademie Verlag, fifth edition.

Massey, P. and Meyer, M. (2001). *Encyclopedia of Astronomy and Astrophysics, Stellar Masses*, pages 4580–4585. Nature Publishing Group.

Murante, G., Calabrese, M., De Lucia, G., Monaco, P., Borgani, S., and Dolag, K. (2012). A Warm Mode of Gas Accretion on Forming Galaxies. *The Astrophysical Journal*, 749:L34.

Peacock, J. A. (1998). *Cosmological Physics*. Cambridge University Press, first edition.

Prialnik, D. (2000). *An Introduction to the Theory of Stellar Structure and Evolution*. Cambridge University Press, first edition.

Schneider, P. (2007). *Einführung in die Extragalaktische Astronomie und Kosmologie*. Springer Berlin Heidelberg, first edition.

Springel, V. (2005). The cosmological simulation code GADGET-2. *Monthly Notices of the Royal Astronomical Society*, 364:1105–1134.

Springel, V., Di Matteo, T., and Hernquist, L. (2005a). Modelling feedback from stars and black holes in galaxy mergers. *Monthly Notices of the Royal Astronomical Society*, 361:776–794.

Springel, V. and Hernquist, L. (2003). Cosmological smoothed particle hydrodynamics simulations: a hybrid multiphase model for star formation. *Monthly Notices of the Royal Astronomical Society*, 339:289–311.

Springel, V., White, M., and Hernquist, L. (2001). Hydrodynamic Simulations of the Sunyaev-Zeldovich Effect(s). *The Astrophysical Journal*, 549:681–687.

Springel, V., White, S. D. M., Jenkins, A., Frenk, C. S., Yoshida, N., Gao, L., Navarro, J., Thacker, R., Croton, D., Helly, J., Peacock, J. A., Cole, S., Thomas, P., Couchman, H., Evrard, A., Colberg, J., and Pearce, F. (2005b). Simulations of the formation, evolution and clustering of galaxies and quasars. *Nature*, 435:629–636.

Tipler, P. A. (1994). *Physik*. Spektrum Akademischer Verlag, first edition.

Tornatore, L., Borgani, S., Dolag, K., and Matteucci, F. (2007). Chemical enrichment of galaxy clusters from hydrodynamical simulations. *Monthly Notices of the Royal Astronomical Society*, 382:1050–1072.

Tornatore, L., Borgani, S., Matteucci, F., Recchi, S., and Tozzi, P. (2004). Simulating the metal enrichment of the intracluster medium. *Monthly Notices of the Royal Astronomical Society*, 349:L19–L24.

Weigert, A., Wendker, H., and Wisotzki, L. (2009). *Astronomie und Astrophysik*. Wiley-VCH Verlag GmbH & Co. KGaA, fifth edition.

Selbstständigkeitserklärung

Hiermit versichere ich,

dass ich diese Bachelorarbeit zum Thema:

'Cold Streams in High-Redshift-Galaxies'

selbstständig verfasst habe. Ich habe keine anderen als die angegebenen Quellen und Hilfsmittel benutzt, sowie Zitate kenntlich gemacht.
Mir ist bekannt, dass Zuwiderhandlung auch nachträglich zur Aberkennung des Abschlusses führen kann.

München,	
Ort, Datum	Unterschrift